

The Arches cluster revisited: IV. Observational constraints on the binary properties of very massive stars[★]

J. S. Clark,¹ † M. E. Lohr,¹ F. Najarro² ‡ L. R. Patrick^{2,3,1} and B. W. Ritchie¹

¹*School of Physical Sciences, The Open University, Walton Hall, Milton Keynes MK7 6AA, UK*

²*Departamento de Astrofísica, Centro de Astrobiología, (CSIC-INTA), Ctra. Torrejón a Ajalvir, km 4, 28850 Torrejón de Ardoz, Madrid, Spain*

³*Departamento de Física Aplicada, Facultad de Ciencias, Universidad de Alicante, Carretera San Vicente s/n, E03690, San Vicente del Raspeig, Spain*

Accepted 2023 February 2

ABSTRACT

Serving as the progenitors of electromagnetic and gravitational wave transients, massive stars have received renewed interest in recent years. However, many aspects of their birth and evolution remain opaque, particularly in the context of binary interactions. The centre of our galaxy hosts a rich cohort of very massive stars, which appear to play a prominent role in the ecology of the region. In this paper we investigate the binary properties of the Arches cluster, which is thought to host a large number of very massive stars. A combination of multi-epoch near-IR spectroscopy and photometry was utilised to identify binaries. 13 from 36 cluster members meet our criteria to be classed as RV variable. Combining the spectroscopic data with archival radio and X-ray observations - to detect colliding wind systems - provides a lower limit to the binary fraction of $\sim 43\%$; increasing to $\gtrsim 50\%$ for the O-type hypergiants and WNLha. Dynamical and evolutionary masses reveal the primaries to be uniformly massive ($\gtrsim 50M_{\odot}$). Where available, orbital analysis reveals a number of short period, highly eccentric binaries, which appear to be pre-interaction systems. Such systems are X-ray luminous, with 80% above an empirical bound of $(L_x/L_{\text{bol}}) \sim 10^{-7}$ and their orbital configurations suggest formation and evolution via a single star channel; however, we cannot exclude a binary formation channel for a subset. Qualitative comparison to surveys of lower mass OB-type stars confirms that the trend to an extreme binary fraction ($\geq 60\%$) extends to the most massive stars currently forming in the local Universe.

Key words: stars: massive – stars: Wolf-Rayet – binaries: spectroscopic

1 INTRODUCTION

Despite their rarity, massive stars are a principal agent in galactic evolution, due to the deposition of mechanical, chemical and radiative feedback. They - and their relativistic descendants - dominate the electromagnetic emission of galaxies at both high (UV and X-ray) and low (IR and radio) energies, the former directly and the latter via reradiation. In both life and death they are thought to be an important source of cosmic rays, while the nature and demographics of gravitational wave sources directly follow from the properties of their stellar antecedents.

Consequently, it is a matter of regret that significant facets of the lifecycle of massive stars remain poorly understood, from their formation mechanism through to their anticipated deaths in either (core-collapse or pair instability) supernovae or direct collapse events. Moreover spectroscopic and imaging surveys of both clustered and isolated OB stars over the past decade have revealed a further com-

plication: that many such objects are to be found in binaries or higher order multiples (Sana et al. (2012), (2013a), (2014), Kobulnicky et al. (2014), Sota et al. (2014), Dunstall et al. (2015), Almeida et al. (2017)). This finding implies significant modification of the already unresolved evolutionary pathways of single stars, driven by tidal interaction, binary mass transfer and, in extreme cases, merger (de Mink et al. (2009), (2014), Schneider et al. (2014)).

Such uncertainty is particularly acute for very massive stars and gives rise to several fundamental and interwoven questions. Is there an upper limit to the mass with which a star may be born? How many such stars are found within hierarchical systems? Do the majority achieve their final mass during formation or instead via binary-driven mass transfer or merger at a later stage (cf. Schneider et al. (2014))? And, at the end of their lives do massive stars evolving via either single or binary channels retain sufficient mass to undergo pair instability supernova and, if not, how does radiative and binary driven mass loss affect the demographics of the resultant neutron star (NS) and black hole (BH) populations?

One region where these uncertainties are manifest is the Central Molecular Zone (CMZ) of the Milky Way. Observations suggest that the properties of the CMZ are particularly extreme, with the mean temperature, density, pressure and velocity dispersion of molecular material, the magnetic field strength and the cosmic ray density and ionisation rate significantly greater than those found in molecular clouds in the Galactic disc, in some cases by orders of magnitude.

[★] Based on observations made at the European Southern Observatory, Paranal, Chile under programmes ESO 087.D-0317, 091.D-0187, 093.D-0306, 099.D-0345 and 0101.D-0141.

† In Memoriam: This work is dedicated to the memory of our dearest friend and colleague Simon Clark. His great enthusiasm pushed all of us to work towards unveiling massive young clusters. The Arches cluster and Westerlund 1 will certainly miss one of their best ambassadors.

‡ E-mail: najarro@cab.inta-csic.es (FN)

An obvious question is therefore whether (massive) stars form in the same manner in this tract as they do in more quiescent regions of the Galaxy. This is of particular importance given that the physical conditions present within the CMZ are anticipated to bear close resemblance to those of starburst galaxies (Kruijssen & Longmore (2013)); hence determining the nature of star formation in the CMZ will provide unique insights into such activity at high redshift.

Based on the numbers of supernova remnants and young neutron stars observed within the CMZ, it must host a population of massive stars of a size capable of yielding one core collapse event every thousand years (Deneva et al. (2009), Kennea et al. (2013), Ponti et al. (2015)). Near-IR imaging and spectroscopy reveal that massive stars are indeed present - albeit not yet detected in the quantities required - and reside in three apparently co-eval massive clusters as well as being distributed, in apparent isolation, throughout the region (e.g. Clark et al. (2018c) and refs. therein).

Of the former cohort, with an age of $\sim 2 - 3$ Myr (Clark et al. (2018a)) the Arches is the youngest of the massive clusters within the CMZ (Figer (1995), Nagata et al. (1995), Cotera et al. (1996)). As a consequence one would not expect it to have lost any stars to core collapse at this juncture; hence the observed population of 13 Wolf-Rayet and ~ 100 O-type stars should reflect the original yield of the star formation process that gave rise to it (Blum et al. (2001), Figer et al. (2002), Martins et al. (2008), Clark et al. (2018a), (2019b)). Moreover, with an integrated mass of $\gtrsim 10^4 M_{\odot}$ (Clarkson et al. (2012)) the upper reaches of the initial mass function (IMF) are richly populated; as such, it provides a unique astrophysical laboratory for the study of the birth channel(s) and physical properties of the most massive stars Nature currently permits to form in the local Universe (Figer (2005)).

In order to exploit this potentiality, between 2011 and 2018 we undertook a new multi-epoch spectroscopic survey of the Arches, reported in an ongoing series of papers. In Clark et al. ((2018a), (2019b); Papers I and III, respectively) we combined multiple epochs to produce spectra reaching stars as faint as O9.5V for the first time in order to produce a cluster census. Quantitative model-atmosphere analysis of these data will facilitate the construction of an HR diagram and the calibration of the luminosity and (initial) mass functions for the cluster. A parallel goal of our programme was to identify massive binaries via radial velocity (RV) variability across epochs in the brightest cluster members, presenting the first example - the eclipsing WN8-9h + O5-6Ia⁺ binary F2 - in Lohr et al. ((2018); Paper II). In this paper we present the results for the remaining cluster members bright enough to permit such analysis. This yields a robust sample size of 36 stars, allowing us to address a number of the outstanding issues regarding the properties and formation of massive binaries ($\gtrsim 40 M_{\odot}$; Sects. 4 and 5) in an extreme physical environment. Moreover, the long observational baseline available to us (Sect. 2) allows us to investigate secular variability in this population.

The paper is therefore structured as follow. In Sect. 2 we define our stellar sample and discuss the spectroscopic and photometric datasets employed in this work. Sect. 3 presents an overview of these datasets and, where appropriate, detailed discussion of individual stars, supplemented by extant radio and X-ray observations. We provide quantitative model-atmosphere analysis of binary candidates in Sect. 4, utilising these to infer current and initial masses for system components. We discuss the implications of these results in Sect. 5 in terms of the binary frequency and properties of very massive stars and, subsequently, the nature of their formation mechanism and evolutionary pathways. Finally we summarise our conclusions in Sect. 6. We also provide three appendices; Sect A.1 provides a comprehensive observational log of our Arches spectroscopic observations;

Sect. B discusses the implications of the lack of secular variability evident in the spectroscopic dataset; Sect. C presents a comprehensive assessment of the binary fraction amongst WNLha stars within stellar clusters and associations and includes a detailed reappraisal of the X-ray properties of single and binary star examples.

2 OBSERVATIONS

2.1 Spectroscopic data and reduction

The SINFONI integral field spectrograph on the ESO/VLT (Eisenhauer et al. (2003), Bonnet et al. (2004)) was used in service mode to make repeated observations of overlapping fields covering the central region of the Arches, and several distinct outlying fields, in the *K* band, in 2011, 2013, 2017 and 2018¹. The long baseline imposed by these multi-semester observations has the advantage of increasing sensitivity to long period systems. Unfortunately, however, the uneven temporal sampling imposed by observations undertaken in service mode complicates future Monte Carlo analysis of the complete dataset.

A further epoch of SINFONI observations for outlying fields from 2005 was furnished by data cubes used for Martins et al. ((2008))². For seven Wolf-Rayet targets, observations were also made in 2014 with KMOS/VLT (Sharples et al. (2013))³, as part of a wider survey of massive stars across the central molecular zone (Clark et al. (2018c)). Lohr et al. ((2018)) also give details of additional archival SINFONI and Keck/NIRSPEC spectra used in the analysis of F2; these are not considered here in the interests of survey consistency.

A detailed account of the acquisition and reduction approach taken for the SINFONI observations is given in Clark et al. ((2018a), (2019b)); for KMOS, details are presented by Clark et al. ((2018c)). For our purposes here, we note particularly that where multiple observations had been made of a science target within the same epoch (in practice, within a few hours of each other on the same night) their spectra were combined to give a higher S/N spectrum. However, distinct epochs were not then combined as described in Clark et al. ((2018a)), because our goal here was the investigation of inter-epoch variability for the brightest objects. The final SINFONI spectra have a spectral resolving power ($\Delta\lambda/\lambda$) of ~ 9000 and cover the wavelength range 2.02–2.45 μm .

2.2 Stellar sample

Multiple epochs of useful spectra were obtained for the majority of Arches sources brighter than F40 (i.e. up to number 40 in the list of Figer et al. ((2002)); objects fainter than this proved to have radial velocity uncertainties comparable in size to their inter-epoch variability. Additionally, stars B1 and B4 (numbers 1 and 4 in the list of Blum et al. (2001)) were confirmed as massive cluster members in Clark et al. ((2018a)), and so were added to the sample. F39 was not included because it was only successfully observed on a single night in 2018 (it lies some distance south of the cluster, and was not surveyed in any previous runs; see Clark et al. ((2019b)) for its spectrum and classification); F31 and 37 are located too close to other, brighter stars for uncontaminated pixels to be extracted; F11 and F36 proved to be cool star interlopers. This leaves a total of

¹ ESO programmes 087.D-0317, 091.D-0187, 099.D-0345 and 0101.D-0141.

² ESO programme 075.D-0736.

³ ESO programme 093.D-0306.

37 stars for which spectra were extracted on at least five epochs. Table 1 summarises statistics on the number of epochs covered for the studied targets, while Table A1 gives the individual dates of observations of each object. Our RV sample consists of thirteen Wolf-Rayet stars (two WN7-8ha and eleven WN8-9ha subtypes), seven O hypergiants (from O4-5 to O7-8Ia⁺; the secondary of F2, classified from disentangled spectra in Lohr et al. ((2018)), is not counted here), and seventeen O supergiants (O4-6.5Ia). Thus, while we are complete for both WNLha stars and O hypergiants we only sample 17/30 of the supergiants (Clark et al. (2019b)).

2.3 Radial velocity measurements

Radial velocities (RVs) were measured by cross-correlation using IRAF's *fxcor* task. To obtain an initial and consistent measure of RV variability for all stars in the sample, in the absence of suitable independent spectral templates, all possible pairs of epochs for a target were cross-correlated with each other. This yielded an $n \times n$ distance matrix, where n is the number of epochs observed, with zeroes along the diagonal where a spectrum was cross-correlated with itself. The sum of each row in this matrix then gave an estimate of the RV of the zero-element in that row, relative to the middle of the range of RVs. The sum of each column gave a second estimate of the RV of the zero-element in that column, multiplied by -1. A simple average was taken of these two estimates for each velocity, and uncertainties were also determined as the average of the uncertainties in the contributing cross-correlation measurements. We refrained from using weighted averages as it was found to bias the results in favour of smaller RVs which could generally be measured more precisely. At this stage, SINFONI and KMOS spectra (where the latter were available) were studied separately, to produce a consistent set of results.

Owing to the range of spectral types of the stars observed, from Wolf-Rayets through O hypergiants to O supergiants, no single set of lines in the *K* band could be used for all targets. For example, in the WNLh spectra, Br γ is the strongest emission line, while C IV lines (2.070–2.084 μm) are weak to non-existent; conversely, in the O supergiants, C IV are the strongest lines, with very weak Br γ due to substantial wind filling of the line. Moreover, many WNLh lines are significantly broadened or show P Cygni profiles associated with wind effects, while in O stars these features are not evident; there is also a significant blended line (He I, N III, C III, O III at 2.112–2.115 μm). For these reasons, fitting of Gaussian or Lorentzian profiles to individual lines was not judged suitable for obtaining RVs across our sample. Cross-correlations were therefore carried out using three overlapping sets of relatively narrow lines:

- (i) He II at 2.037 and 2.189 μm , and N III at 2.247 and 2.251 μm for all WNLh targets;
- (ii) The same lines as in (1) with the addition of C IV at 2.07–2.084 μm for a subset of WNLh stars in which these lines are stronger;
- (iii) He I at 2.058 μm , C IV at 2.07–2.084 μm , the blend at 2.112–2.115 μm , and He II at 2.189 μm for the O hypergiants and supergiants.

Given our use of observed spectra of each target as templates, our RVs are necessarily relative rather than absolute. However, our approach to detecting variability in a target relies upon the maximum significance of an RV difference between any two pairs of epochs, as

used by various authors (Sana et al. ((2013a)), Dunstall et al. ((2015)), Patrick et al. ((2019), (2020)), Ritchie et al. ((2021)):

$$\sigma_{\text{det}} = \max \left(\frac{|v_i - v_j|}{\sqrt{\sigma_i^2 + \sigma_j^2}} \right), \quad (1)$$

where $v_{i,j}$ and $\sigma_{i,j}$ are the RVs and their associated uncertainties at epoch i or j . Therefore, absolute RVs are not required.

In order to identify variability associated with likely binarity, Sana et al. ((2013a)) required stars to exhibit both $\sigma_{\text{det}} > 4.0$ and at least one pair of measurements from distinct epochs to satisfy $|v_i - v_j| > 20 \text{ km s}^{-1}$. The former criterion ensures minimal false positives; important given the combination of large sample size but comparatively low observational frequency of their study. The latter threshold was chosen to minimise contamination from pulsating sources within the sample and was motivated by the behaviour of blue super-/hypergiants within Westerlund 1 (Ritchie et al. (2009)). A higher 25 km s^{-1} threshold is adopted by Ritchie et al. ((2021)) to accommodate the larger pulsational amplitudes observed in the early-B supergiant population of Westerlund 1, but these later-type objects are not present in the Arches. Foreshadowing Sect. 3, we find no evidence for secular variability in the spectral morphologies of our targets, as is observed in the lower-mass blue super-/hypergiant contingent within Westerlund 1 (Ritchie et al. (2009), Clark et al. (2010)), and we regard the 20 km s^{-1} threshold adopted by Sana et al. ((2013a)) as appropriate for this study.

The situation for the WNLh stars is different as the emergent emission line spectrum originates in an optically thick wind; as a consequence we would not expect to observe pulsationally driven line profile variability. However, a number of studies have revealed modification of line profiles in (apparently) single WRs due to the presence of both small-scale wind clumping and large-scale rotating structures (e.g. Lépine & Moffat (1999), St-Louis et al. (2009)). However the effect of the former is the superposition of additional, small sub-peaks on the stationary emission profile (Lépine & Moffat (1999)) - which would not be expected to introduce global RV shifts. Fortunately, globally structured winds are only seen in a small subset of WRs, none of which are of comparable spectral types to the Arches cohort (St-Louis et al. (2009)), while this phenomenon does not impart motion to the whole emission profile. For completeness, Stevens & Howarth ((1999)) report significant line profile variability in WR colliding wind binaries, but clearly we would not wish our detection threshold to exclude such systems. Nevertheless, the potential for line profile variability to be ubiquitous amongst WRs still requires us to choose an appropriate velocity cut for such stars. Fortunately, Schnurr et al. ((2008a), (2009a)) searched for binaries amongst the WNLh cohort of both NGC3603 and R136 with an identical experimental set up (VLT/SINFONI) and wavelength range (*K*-band) to that employed in this study, finding that apparently single stars showed random variability of $\Delta\text{RV} < 20 \text{ km s}^{-1}$.

Therefore, upon consideration of the above, we adopt thresholds of $\sigma_{\text{det}} > 4.0$ and $|v_i - v_j| > 20 \text{ km s}^{-1}$ for binarity for both the WNLh stars and O super-/hypergiants within the Arches, allowing direct comparison to the studies highlighted above. After an initial identification of candidate binaries via these criteria, RVs were measured again for each species individually, to assess the most useful lines for determining precise velocities; moreover, the combined spectra of non-variable Arches members with identical or very similar classifications were used as templates for cross-correlation. Orbital periods were then sought, using both Lomb-Scargle periodograms (Lomb

(1976), Scargle (1982), Horne & Baliunas (1986)) and a form of string length minimization (Dworetzky (1983)).

Given the limitations of our dataset in terms of sampling, false periods arising from noise and aliasing may be problematic. In order to address this issue we employed $k - 1$ cross validation to assess the reality of any periodicities returned. In each resampled subset false periods in the periodogram are expected to vary in strength and/or location, while a peak resulting from the true orbital period will be robust against such a test, providing confirmation of its physical nature.

2.4 Photometry

K_s band time-series photometry of the Arches cluster (excluding B1 and F39) was obtained by Pietrzynski et al.⁴ between 2008 and 2009 using NAOS-CONICA (NaCo) on the VLT (Lenzen et al. (2003), Rousset et al. (2003)). This study was briefly reported in Markakis ((2011), (2012)). We reprocessed the raw archival data as described in Lohr et al. ((2018)), and thus generated light curves for the brighter objects which were present in all observations. Non-variable sources were identified and combined to provide a composite reference star, relative to which differential light curves could be constructed for variable objects.

3 DATA PRESENTATION AND RESULTS

We present the results of our initial RV variability measurements - determined independently for SINFONI and KMOS observations - in Table 1. Before discussing these data in detail we briefly note that none of the 37 targets showed evidence for long term, secular spectral variability; we discuss this observational finding and the implications in Section 5.1 and Appendix B.

It proved possible to obtain ΔRV values for all members of the sample except F19, which is a close neighbour of the much brighter (and photometrically variable) F2 (Lohr et al. (2018)). As a consequence we suspect the spectra of F19 were contaminated by F2 to varying extents in different epochs: its cross-correlation function was not well-defined for any pairs of its five epochs of spectra. A few other objects had one or more epochs which proved to be strong RV outliers. While these could derive from highly eccentric binaries, such measurements generally corresponded to poorer-quality observations with much larger uncertainties than the other epochs; as such we proceed under the assumption that these values are spurious. The ΔRV values obtained after removal of these presumed outliers are also given in Table 1, and are used for subsequent analysis.

Fig. 1 shows the distribution of the measured objects in $\Delta RV - \sigma_{\text{det}}$ space and their location with respect to the thresholds for binarity we adopted: $\sigma_{\text{det}} > 4.0$ and $|v_i - v_j| > 20 \text{ km s}^{-1}$. F2 stands out as exhibiting the greatest amplitude of variability ($\Delta RV \sim 360 \text{ km s}^{-1}$) and the highest significance ($\sigma_{\text{det}} \sim 33$) of the SINFONI measurements, and the only significant result determined from the KMOS dataset in isolation. No other object provides such clear-cut evidence; however, thirteen targets meet our criteria for significant variability suggestive of binarity: 6/13 WNLh stars, 2/7 O hypergiants and 5/16 O supergiants (Table 1). This suggests an RV-derived binary fraction of 13/36 ($\sim 36\%$) before any correction for observational biases. As described in Sect. 2.3, the choice of $\sigma_{\text{det}} > 4.0$ reflects our desire to limit false positive detections in the dataset; that being said, given the

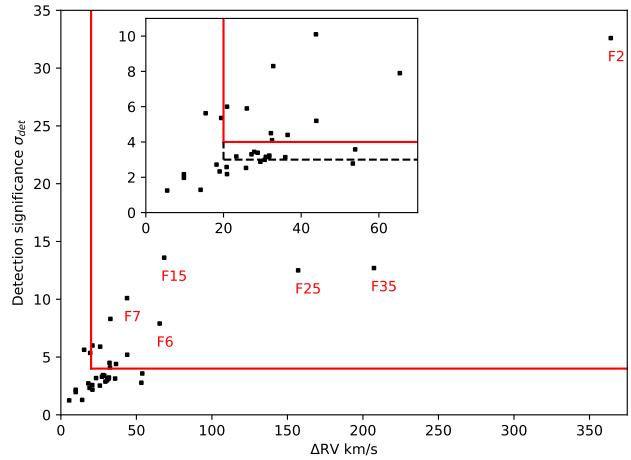


Figure 1. Distribution of ΔRV against σ_{det} for 36 bright Arches members. Our thresholds for significance and amplitude of variability suggesting binarity are marked with solid red lines. Stars for which searches for orbital solutions have been attempted are labelled. The inset shows in more detail the majority of our targets. The black dashed line shows a less conservative, $\sigma_{\text{det}} > 3.0$, threshold for binary detection.

sample size, statistically, one would also expect 0 false positives assuming $\sigma_{\text{det}} > 3.0$ as a threshold for binarity. In this scenario, 22/36 ($\sim 61\%$) meet the RV variability criteria for binarity. This additional subset consists of 1 WNLh star, 2 O hypergiants and 6 O supergiants.

In addition to F2, the amplitude of RV variability of five cluster members - F6, F7, F15, F25, and F35 - is sufficient to attempt a provisional determination of their orbital parameters. These stars are discussed individually in Sect. 3.1. While the remaining seven sources - F8, F14, F16, F18, F28, F29, and F32 - are also *bona fide* RV variables, a combination of fewer epochs of observations and lower amplitude RV excursions precluded the identification of periodicities at this time. In the case of the supergiant cohort these limitations are compounded by their weaker spectral features and lower S/N spectra. Despite their RV variability we highlight that none of these latter sources appear to be SB2 binaries, nor do they show evidence for line profile variability indicative of binarity.

In the case of the RV variables with $3.0 < \sigma_{\text{det}} < 4.0$, F40 stands out with $\Delta RV \sim 54 \text{ km s}^{-1}$ and 15 epochs. Analysis of this system strongly suggests that it is also a short-period binary, but, given the larger uncertainties for the RV measurements for this target (see Table A1), determination of orbital parameters would require further observations.

No further eclipsing or periodically varying systems were identified in the photometric dataset analysed; where appropriate these data are discussed below for individual objects. Finally we may make use of additional, extant X-ray and radio observations to identify further binaries; these datasets - and the conclusions deriving from them - are discussed in Sect. 3.3.

3.1 Individual sources

3.1.1 F6

F6 (WN8–9ha) is perhaps the brightest source in the Arches, and is projected against the cluster core. He II lines at 2.037, 2.189 and 2.346 μm and C IV lines at 2.070 and 2.078 μm were used to determine RVs, and F1 was selected as a cross-correlation template:

⁴ ESO proposal 081.D-0480.

Table 1. RV variability results for Arches members, ordered by spectral classification.

Star ref.	Spectral Type	ΔRV (km s ⁻¹)	σ_{det}	Line set	No. of epochs	X-ray detection?	Radio properties	Alt. Star ref.
B1	WN8-9ha	5.5 <i>16.1</i>	1.25 <i>1.72</i>	1	5 7		thermal	WR 102bc
F1	WN8-9ha	20.9 <i>5.9</i>	2.18 <i>1.34</i>	2	14 2		thermal, variable	WR 102ad
F2	WN8-9ha	364.1 <i>280.7</i>	32.61 <i>17.31</i>	1	6 7	•	composite	WR 102aa
F3	WN8-9ha	9.8	1.97	1	7		thermal	WR 102bb
F4	WN7-8ha	19.4	5.36	1	10		thermal	WR 102al
F5	WN8-9ha	15.4	5.63	1	7		composite, variable	WR 102ai
F6	WN8-9ha	65.4 <i>54.2</i>	7.99 <i>2.99</i>	2	10 7	•	composite, variable	WR 102ah
F7	WN8-9ha	43.8	10.12	1	15	•	thermal, variable	WR 102aj
F8	WN8-9ha	20.9 <i>14.9</i>	6.05 <i>1.40</i>	1	10 7		thermal	WR 102ag
F9	WN8-9ha	27.9 <i>13.6</i>	3.44 <i>1.00</i>	2	15 6	•	composite, variable	WR 102ae
F12	WN7-8ha	19.0	2.33	2	10		non-thermal	WR 102af
F14	WN8-9ha	32.8	8.39	2	11		unconstrained	WR 102ba
F16	WN8-9ha	26.0	5.90	2	10		unconstrained	WR 102ak
F10	O7-8 Ia ⁺	9.8	2.17	3	10		-	[BSP2001] 30
F13	O7-8 Ia ⁺	29.5	2.88	2	9		-	[BSP2001] 31
F15	O6-7 Ia ⁺	68.4	13.66	3	16		-	[BSP2001] 8
F17	O5-6 Ia ⁺	18.2	2.72	2	10		-	[BSP2001] 29
F18	O4-5 Ia ⁺	32.2	4.56	3	10		non-thermal, variable	[BSP2001] 20
F27	O4-5 Ia ⁺	30.9	3.16	3	14		-	[BSP2001] 16
F40	O4-5 Ia ⁺	53.9	3.58	3	15		-	-
B4	O5.5-6 Ia	23.3	3.18	3	11		-	-
F19	O4-5 Ia	-	-	3	5		non-thermal	[LGR2001] AR6
F20	O4-5 Ia	30.6	2.99	3	14		-	-
F21	O6-6.5 Ia	31.7	3.15	3	15		-	[BSP2001] 7
F22	O5.5-6 Ia	27.2	3.30	3	9		-	[BSP2001] 27
F23	O6-6.5 Ia	20.8	2.58	3	6		-	[BSP2001] 2
F24	O4-5 Ia	25.8	2.53	3	5		-	-
F25	O4-5 Ia	157.1	12.51	3	12		-	-
F26	O4-5 Ia	53.3	2.78	3	8		unconstrained	[BSP2001] 18
F28	O4-5 Ia	32.5	4.15	3	10		-	-
F29	O5.5-6 Ia	36.5	4.48	3	16		-	[BSP2001] 9
F30	O4-5 Ia	14.1	1.29	3	8		-	-
F32	O4-5 Ia	43.9	5.24	3	10		-	[BSP2001] 15
F33	O4-5 Ia	35.9	3.14	3	10		-	[BSP2001] 13
F34	O4-5 Ia	31.8	3.23	3	10		-	[BSP2001] 5
F35	O4-5 Ia	207.3	12.74	3	16		-	[BSP2001] 10
F38	O4-5 Ia	28.8	3.39	3	9		-	-

Rows in italics correspond to KMOS observations. Values in bold face meet our criteria for significant variability associated with likely binarity. X-ray detections given by bullet points in column 7 (Wang et al. (2006)). Radio properties of individual stars derived from Lang et al. ((2001), (2005)) and Gallego-Calvente et al. ((2021)) are summarised in column 8; thermal sources are those with spectral indices consistent with expectations for a partially optically thin wind ($\alpha \sim 0.6$), non-thermal sources demonstrate $\alpha < 0.0$, while composite sources lie between these extremes (Sect. 3.3). Three stars are only detected at one frequency; hence their spectral indices are unconstrained. Note that the targets can be accessed in SIMBAD via column one by replacing ‘F’ with ‘[FNG2002]’, or ‘B’ with ‘[BSP2001]’.

this object is also classified as WN8-9ha and exhibits a very similar appearance to F6 in terms of line strengths and profiles, but does not exhibit significant RV variability.

We find $\Delta RV \sim 65 \text{ km s}^{-1}$ and $\sigma_{\text{det}} \sim 8$ from ten SINFONI spectra, while seven KMOS spectra from 2014 independently yield $\Delta RV \sim 55 \text{ km s}^{-1}$. Fig. 2 shows the RV curve derived from the He II

line set, folded to a period of 13.378 ± 0.004 days derived from a string-length search⁵. We find a full amplitude of $\sim 50 \pm 5 \text{ km s}^{-1}$

⁵ No periods with false-alarm probabilities below 10% were found using the Lomb-Scargle method; this is perhaps unsurprising given that the RV curve appears strongly non-sinusoidal in shape

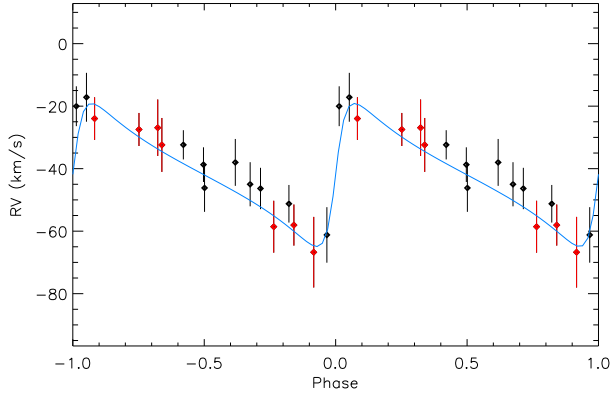


Figure 2. RV curve for F6, cross-correlated relative to F1, measured from three spectral regions containing He II lines, folded on $P=13.378$ d. RVs and uncertainties from SINFONI spectra are shown in black; those from KMOS are shown in red. The blue line corresponds to a possible model system with $e=0.6$, $\omega=270^\circ$.

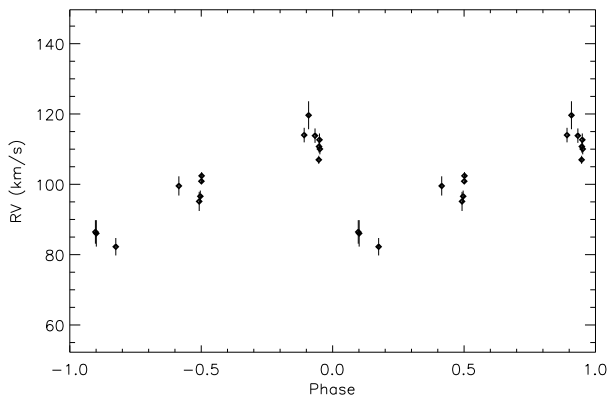


Figure 3. SINFONI RV curve for F7, cross-correlated relative to F5, measured from the Br γ line, and folded on $P=1184.46$ d.

and orbital eccentricity $e \sim 0.6$. Similar results are obtained from the C IV line set, the strong blended feature at $2.112\text{--}2.115 \mu\text{m}$, and a combination of C IV lines, He II at $2.189 \mu\text{m}$ and N III at 2.247 and $2.251 \mu\text{m}$. Checks were also made using F5 (another relatively RV-invariant WN8-9ha star) as a template, yielding consistent, if somewhat noisier, results.

This solution suggests a relatively low-mass companion, and/or a moderate angle of inclination, which may in turn explain why F6 exhibits relatively little photometric variability and no significant periodicity in its light curve. There is, however, possible evidence for line profile variability, with weaker Br γ and a less marked P Cygni profile for the He II $2.189 \mu\text{m}$ line in a maximum-RV spectrum, as compared with a phase 0 spectrum, in which both components' features would be expected to be aligned. Nevertheless, the RV data presented here strongly support the identification of F6 as a massive binary, and its high eccentricity would imply a pre-interaction system.

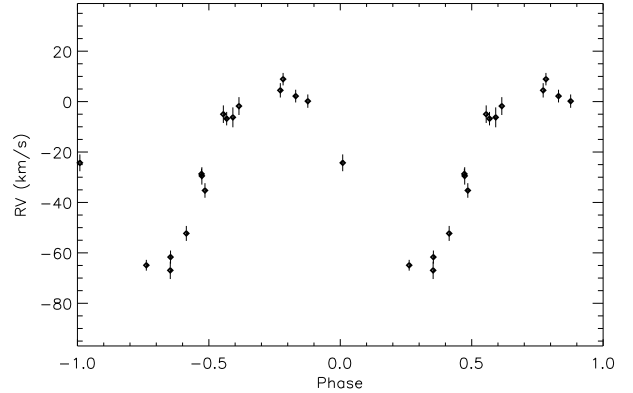


Figure 4. SINFONI RV curve for F15, cross-correlated relative to F10, measured in the region of the blended spectral feature at $2.112\text{--}2.115 \mu\text{m}$, and folded on $P=83.95$ d.

3.1.2 F7

F7 is another very bright WN8-9h star in the cluster core. RVs were measured using F5 as a template, and cross-correlating over a range of discrete wavelength regions. The best results were produced by the very strong Br γ line, revealing variability with a significance of $\sigma_{\text{det}} \sim 10$ and an amplitude of $\sim 40 \text{ km s}^{-1}$. It is notable that the RVs within each season of observation are very similar⁶, implying a long period system and effectively reducing to three the number of separate RV measurements; systematic errors can be excluded, as other nearby bright targets extracted from the same data cubes do not exhibit the same RV shifts. The orbital period is not well constrained by the current data; the shortest plausible period is around 3.24 years (see Fig. 3), but the true period may be significantly longer given the degeneracies in the interpretation of the RV curve with three effective RV measurements, which means that longer orbital periods are also possible. Photometric data shows very little variability (0.05 mag), and there are also no obvious line profile changes between seasons.

3.1.3 F15

F15 (O6-7 Ia⁺) lies near the centre of the cluster, and has the second highest detection significance evidence in our sample. Like the other O hypergiants in the Arches, F15's spectrum exhibits a number of relatively strong and narrow features, especially the C IV lines at 2.070 and $2.078 \mu\text{m}$, He I at $2.059 \mu\text{m}$, and the blend at $2.112\text{--}2.115 \mu\text{m}$ (Sect. 4). Improved RVs were determined in these wavelength regions using F10 (O7-8 Ia⁺) as a template, since it showed very little evidence for variability itself; F17 (O5-6 Ia⁺) was also used as a check comparator.

Period searches using both Lomb-Scargle and string length minimization approaches give a period of 83.9 days with false-alarm probability $< 1\%$. The cleanest folded RV curve (shown in Fig. 4) was produced using the blend region at $2.112\text{--}2.115 \mu\text{m}$, with the C IV lines also producing a very similar result. Using these two sets of RVs, we converged on a best consensus period of 83.95 ± 0.15 days. The RV curve is approximately sinusoidal, and has a full amplitude around $75 \pm 5 \text{ km s}^{-1}$. No notable line profile changes are observed

⁶ F7 was observed seven times in 2013, three times in 2017, and five times in 2018.

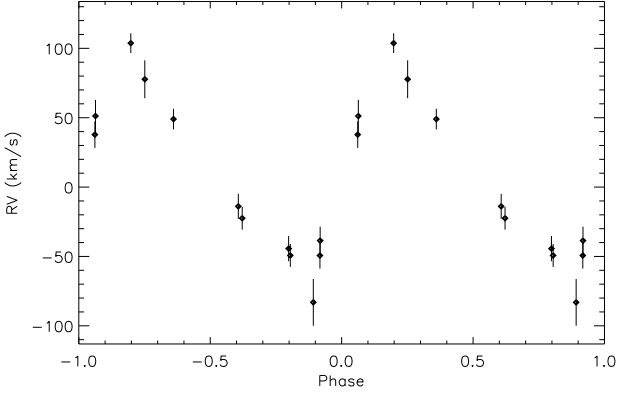


Figure 5. SINFONI RV curve for F25, cross-correlated relative to F23, measured in the regions $\sim 2.05\text{--}2.13\ \mu\text{m}$ and $2.18\text{--}2.20\ \mu\text{m}$, and folded on $P=6.643\ \text{d}$.

across the orbital cycle. F15 is a low amplitude photometric variable ($\sim 0.06\ \text{mag}$), with no evidence of periodic modulation, which is unsurprising given its period and the limited duration and temporal sampling of the dataset. The orbital period of nearly three months suggests a detached pre-interaction system, with the relatively low amplitude and lack of photometric or line profile variability suggesting that the secondary is of lower mass and luminosity, and/or low inclination.

3.1.4 F25

F25 (O4-5 Ia) is located southwest of the cluster core in the vicinity of F2. Like the other O supergiants, it is less luminous than the WNLs and O hypergiants in the cluster, and its spectral features are relatively weak; consequently the individual epochs are noisier, making it more difficult to obtain reliable RVs. F23 was selected as a template and the regions $\sim 2.05\text{--}2.13\ \mu\text{m}$ and $2.18\text{--}2.20\ \mu\text{m}$ were included in the cross-correlation in order to improve RV measurement.

The most compelling orbital solution, shown in Fig. 5, suggests a period of 6.643 ± 0.002 days, with pronounced eccentricity ($e = 0.35 \pm 0.09$) and a full amplitude of $\sim 165 \pm 15\ \text{km s}^{-1}$, although an alternative candidate period of ~ 5.45 days with similar eccentricity and amplitude cannot be excluded⁷. Both solutions imply a pre-interaction system with a massive companion. F25 exhibits a moderate degree of photometric variability ($\sim 0.2\ \text{mag}$), but no obvious periodicity was detected in its light curve. Further high S/N observations will be required to provide a unique solution.

3.1.5 F35

Classified as O4-5 Ia and lying near the centre of the cluster, F35 is only slightly brighter than F25 and hence exhibits similar limitations in determining reliable RVs. F23 was again used as a template, with the same wavelength regions for cross-correlation as were adopted for F25.

A best-fit period of 6.043 ± 0.003 days was found, with eccentricity 0.44 ± 0.06 and a full amplitude $260 \pm 10\ \text{km s}^{-1}$ that is the second

⁷ A number of other candidate periods below ten days have false-alarm probabilities 5–10%.

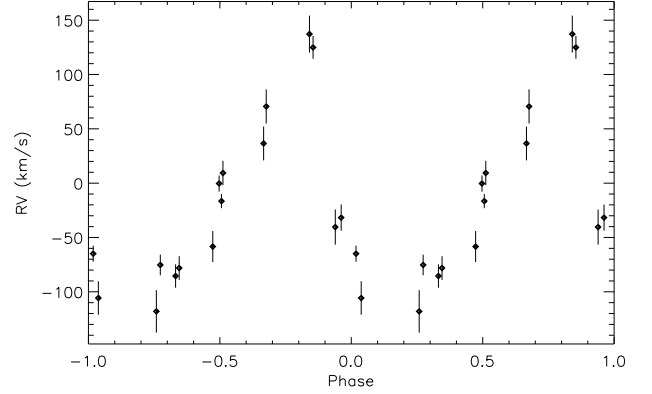


Figure 6. SINFONI RV curve for F35, cross-correlated relative to F23, measured in the regions $\sim 2.05\text{--}2.13\ \mu\text{m}$ and $2.18\text{--}2.20\ \mu\text{m}$, and folded on $P=6.043\ \text{d}$.

largest in our sample, after F2. This solution is plotted in Fig. 6. Unlike F25, no strong alternative candidate periods are found. F35’s photometric variability is limited (0.08 mag) and shows no obvious periodicity near six days. However, comparison of spectral line profiles from observations made during the assumed secondary eclipse and the two quadratures of the proposed $\sim 6.043\ \text{d}$ orbital period does suggest a consistent shape difference: when the two assumed binary components have a common RV (around phase 0.5), the profile is narrower than at either quadrature (when the components are maximally separated in wavelength).

Although further epochs would be desirable to confirm the period of F35, its very large amplitude of RV variability and phase-dependent line profile changes support its identification as another eccentric, short-period massive binary in the Arches. The broadening of spectral lines at quadratures suggests that the companion is of similar spectral type to the O supergiant primary; the high RV amplitude also supports a companion of comparable mass to the primary.

3.2 Ancillary radio and X-ray observations

While spectroscopic and photometric methodologies provide robust binary detections, other indirect diagnostics also exist. Specifically, shocks in the wind collision zones of massive binaries produce high temperature plasma that leads to excess hard, thermal X-ray emission over that expected from single stars (Stevens et al. (1982), Pittard & Dawson (2018)) as well as a population of relativistic electrons that yield non-thermal synchrotron emission at radio wavelengths (Williams et al. (1990), Chapman et al. (1999), Dougherty & Williams (2000), Van Loo et al. (2006)).

3.2.1 X-ray observations

Wang et al. ((2006)) report four X-ray detections of WNLha stars within the Arches: F6 (=A1S; $L_X = 1.1 \times 10^{34}\ \text{ergs}^{-1}$, $kT \sim 2.2^{+0.4}_{-0.3}\ \text{keV}$), F7 (=A1N; $L_X = 7.2 \times 10^{33}\ \text{ergs}^{-1}$, $kT \sim 1.8^{+0.2}_{-0.2}\ \text{keV}$), F9 (=A2; $L_X = 4.6 \times 10^{33}\ \text{ergs}^{-1}$, $kT \sim 2.5^{+0.4}_{-0.3}\ \text{keV}$), and F2 (=A6; no analysis undertaken)⁸. Unfortunately, presumably due to a

⁸ While finding an acceptable single temperature fit to the spectra, Wang et al. ((2006)) report that a two temperature fit comparable to that employed for

combination of the compact nature of the cluster and the spatially variable diffuse background emission, no upper limits were provided for the remaining cluster members.

As described previously, F2, F6 and F7 all appear *bona fide* binaries by virtue of their RV variability. Our extensive RV observations of F9 (15 SINFONI epochs from 2005, 2011, 2013, 2017 and 2018, and 6 KMOS epochs from 2014) revealed no evidence for variability, while it is a low amplitude (< 0.04 mag) aperiodic photometric variable. Nevertheless, foreshadowing discussion of its radio data (Sect. 3.2.2), we conclude that F9 is a massive colliding wind binary due to the similarity of its X-ray properties to those of F2, F6, and F7 (and indeed other confirmed WNLha binaries; Appendix C), with the lack of reflex motion potentially due to an unfavourable orbital inclination.

A number of other WNLha stars that appear strong binary candidates - for example the RV variables F8, F14, and F16 - are not detected as X-ray sources. One might suppose these non-detections derive from either environmental issues (i.e. source blending/confusion in the confines of the cluster) or the intrinsic properties of the binaries themselves. Specifically, while hard, overluminous X-ray emission has traditionally been adopted as a key colliding wind diagnostic, Oskinova ((2005)) and Rauw et al. ((2015)) suggest that not all such systems conform to this expectation. We discuss this further in Appendix C, but note that this assertion is exemplified by observations of Westerlund 1 (Clark et al. (2019c)), where binaries may (i) exhibit the properties of single stars, (ii) be soft X-ray sources that are overluminous with respect to expectations for the primary or (iii) appear as ‘canonical’ hard, overluminous sources; we note, however, that the hardest and brightest X-ray detections remain predominantly binaries. One might suppose that the X-ray properties of colliding wind systems are a sensitive function of both the nature of the stellar components (specifically wind momenta) and orbital configuration (separation and eccentricity); this is particularly important in the context of the Arches, where the extreme column density to the cluster would preclude detection of binaries exhibiting soft X-ray spectra, even if significantly overluminous.

3.2.2 Radio observations

The Arches cluster has been the subject of three radio surveys of increasing sensitivity (Lang et al (2001), (2005) and Gallego-Calvente et al. (2021)). In total 16 cluster members have been detected across these studies, with their properties summarised in Table 1. Following Wright & Barlow ((1975)) thermal emission from a partially optically-thick, isothermal stellar wind should have a characteristic spectral index, $\alpha \sim 0.6$ (where $S_\nu \propto \nu^\alpha$), with increasing optical depth leading to a steepening spectrum. Conversely, non-thermal emission will have a negative spectral index, $\alpha < 0.0$, with composite sources comprising both thermal and non-thermal components being intermediate between these extremes. Following this taxonomy, the radio emission associated with six stars appears thermal in origin (B1, F1, F3, F4, F7, and F8), composite in four (F2, F5, F6, and F9), non-thermal in three (F12, F18, and F19) and unconstrained for

the comparable Galactic Centre binary CXO J1745-28 (Table 3; Mikles et al. (2006), Clark et al. (2009)) would lead to an increase in flux by over an order of magnitude. The extreme sensitivity of X-ray luminosity to the model assumed is a result of the large column density towards Galactic Centre sources; as such, we consider the luminosities adopted for these systems to be lower limits. Moreover this finding also acts as a caution when comparing the properties of sources modelled with different assumptions and also stars observed at very different absorption columns (cf. Table C1).

the remaining three sources (F14, F16, and F26), which were only detected at a single frequency.

We first consider the apparently thermal sources, and of these none show evidence for binarity with the sole exception of F7, which is a confirmed binary by virtue of RV variability and X-ray emission. F7 is an important exemplar since it is known that massive binaries can be radio-variable, with occultation of the wind collision zone at certain orbital phases leading to varying fluxes and spectral indices; indeed such sources sometimes present as thermal in origin (cf. WR140; Williams et al. (1990)). As such, we may not immediately conclude that the remaining thermal sources within the Arches are single stars; in this regard it is notable that Lang et al. ((2005)) report F1 as radio-variable (although this behaviour could also arise from changes in wind properties).

Turning next to the composite systems, F2 and F6 are unambiguously binary, while F9 is a bright, hard X-ray emitter - we consider the combination of X-ray and radio properties for this source as strong evidence for binarity, further noting that Gallego-Calvente et al. ((2021)) report it to be radio-variable. Finally, no evidence for RV variability is visible in the seven epochs of observations of F5; therefore despite the variable, composite nature of its radio emission we refrain from concluding a binary nature for it at this juncture.

F12, F18, and F19 all appear strong binary candidates on the basis of their non-thermal emission, with Gallego-Calvente et al. ((2021)) further noting that F18 appears radio-variable. Our spectroscopic survey reveals that F18 is also RV-variable, while insufficient data exists to draw any conclusions for F19 and no evidence for variability exists in the 12 epochs of observations of F12. Finally, we appraise the three stars displaying unconstrained spectral indices. Both F14 and F16 appear to be binaries on the basis of RV variability, although their radio fluxes are consistent with expectations for emission originating solely in their stellar winds (Martins et al. (2008), Gallego-Calvente et al. (2021)). Conversely no evidence for binarity exists for F26; however the mass loss rate inferred from its radio flux is significantly in excess of that expected for a star of its spectral type. Hence we suspect that a non-thermal component may be present and that it is also a colliding wind binary (with a similar discrepancy observed for the confirmed binaries F6 and F18; Gallego-Calvente et al. (2021)).

3.3 Synopsis

From a sample of 37 objects our spectroscopic survey has identified a total of 13 RV variable cluster members that, as a consequence, are strong binary candidates (Table 1). To these we may add F9 on the basis of its combined X-ray and radio properties, and the non-thermal sources F12 and F19, while three further stars - F1, F5 and F26 - possess radio properties that are, at a minimum, consistent with binarity. Excluding the latter three stars at this point implies a conservative minimum binary fraction for the sample of $\geq 43\%$, noting that no correction has been applied to the spectroscopic survey to account for differences in observational cadences for individual stars, nor the lack of sensitivity to high-inclination systems.

While the spectroscopic survey is complete for the 13 WNLha stars and seven O hypergiants, 14 of the fainter cluster supergiants were excluded due to their lower S/N spectra; given that binaries are likely to be overluminous this potentially introduces an observational bias. Likewise while all stars are expected to be massive ($\geq 40M_\odot$; Sect. 4 and Clark et al. (2018a)), we expect the most luminous WNLha stars to be considerably more massive than the faintest supergiants (cf. Lohr et al. (2018)). Consequently, one would expect them to support stronger winds which might be expected to aid in the detection of emission deriving from wind collision shocks, introducing another

bias. As such, it is instructive to consider the binary fractions for the homogeneous and complete subsets of WNLha stars and O hypergiants, finding them to be $\geq 62\%$ and $\geq 29\%$ respectively, which yields a combined binary fraction of $\geq 50\%$ for this cohort (noting that these numbers exclude the WNLha stars F1 and F5). We discuss these values further in Sect. 5, where we place them into a wider context.

4 MODEL ATMOSPHERE ANALYSIS

We carried out a quantitative spectroscopic analysis of these five systems to address three issues relevant to their binary nature. Firstly we searched for signatures of previous or ongoing binary interaction, such as the simultaneous presence of enhanced carbon and nitrogen (cf. HD 153919 and Wd1-13; Clark et al. (2002), (2014)). Secondly, we checked for subtle observational signatures of the secondary. Finally we sought to obtain evolutionary masses and other fundamental properties for the dominant component(s) of each binary. To model the stars we followed the procedure presented in Lohr et al. ((2018)) making use of two grids (one for WNL and one O-stars) created with CMFGEN (Hillier & Miller (1998), (1999)). In their analysis of the F2 system Lohr et al. ((2018)) were able to undertake spectroscopic disentangling, allowing them to analyse each component separately. However, this was not possible for the five systems in question, and so we modelled the mean of their stacked spectra (once corrected from radial velocity shifts).

We made use of the line profiles of H, He, C, N, O and Si present in the K-band spectra of the objects together with the observed photometry to constrain their stellar properties (e.g. Najarro et al. (2004), Martins et al. (2008) and Lohr et al. (2018)). The effective temperature was obtained from the He II/He I ionization balance by means of the He II 2.037, 2.189 and 2.346 μm and the He I 2.059 μm , and 2.112-3 μm line profiles. The relative strength between the He and Br γ lines was utilized to constrain the He/H fraction while the mass-loss rate was inferred from their absolute strengths. For the WNL stars, the terminal velocity is obtained from He I 2.059 μm , while the full Br γ profile constrains β and its red emission determines the clumping factor, f . For the OIf⁺ star we find a degeneracy between v_∞ and f and adopt a value of $f=0.1$. In the case of the two OIf objects we fixed f and v_{inf} (see Table 2). The N III diagnostic lines at 2.103, 2.115, 2.247 and 2.251 μm together with the N IV/Si IV feature at ~ 2.43 (Clark et al. (2018a)) constrain quite well the nitrogen abundance (Najarro et al. (2004)) specially for the WNLs (see Table 2). The carbon content is obtained from the C IV lines at 2.070 and 2.078 μm . The emission component of the strong He I/C III/N III/O III blend at 2.112–2.115 μm is expected to be dominated by nitrogen in the WNL stars and by oxygen in the O stars (Geballe et al. (2006)). Therefore, when combined with the rest of diagnostic K-band lines it constrains quite well the oxygen abundance of the O stars while providing just an upper limit for the WNLs.

To estimate the system luminosities, we utilised the HST photometry compiled in Clark et al. (2018a) and performed Levenberg-Marquardt fits for different extinction prescriptions scaling the SEDs from the spectroscopic modelling. The availability of six different photometric measurements between 1.0 and 2.5 μm enable a study of a wavelength-dependence of the extinction curve. This has been explored by Lohr et al (2018) in their analysis of F2 and investigated by Nogueras-Lara et al. (2020) for their extinction map of the Galactic Centre. Based on the analysis of our full Arches data sample and the resulting location in the HR diagram of all cluster members (Najarro et al, in prep.) we opted finally for a two- α extinction law of the

form $A_\lambda = A_{k0} \left(\frac{\lambda_{k0}}{\lambda}\right)^\alpha$ where $\alpha = \alpha_1 + \frac{(\alpha_2 - \alpha_1)}{(\log \lambda_2 - \log \lambda_1)} (\log \lambda - \log \lambda_1)$ with α_1 and α_2 defined at λ_1 and λ_2 in the J and K bands respectively. In our case we chose $\lambda_1 = 1.282$ and $\lambda_2 = 2.166$ and obtained $\alpha_1 = 1.79$ and $\alpha_2 = 1.600$. This extinction law results in luminosities roughly ~ 0.25 dex below those which are obtained with the Moneti et al. ((2001)) law and ~ 0.4 dex above those derived with a $\alpha = 2.3$ law approach (Nogueras-Lara et al. (2018)).

4.1 System properties and comparison to previous analyses

Stellar properties of the two WN9h (F6 & F7), the O-hypergiant (F15) and the two O-supergiants (F25 & F35) are presented in Table 2. For each of the objects the first line provides the stellar parameters assuming the two- α extinction law from above, while the second and third rows display the A_K , luminosity, radius and mass-loss rates obtained employing Moneti's and $\alpha = 2.3$ extinction laws respectively. A deeper, more detailed analysis of the stellar properties of these systems will be presented in a future work, where a study of the whole Arches sample will be discussed.

The resultant spectral fits for the WNLh stars (F6 & F7) and the O-stars (F15, F25, & F35) are displayed in Fig. 7 and Fig. 8 respectively. The excellent fits with a single atmospheric model of the full systems support our previous claims of either less massive companions (F6, F7 and F15) or systems of comparable mass and similar spectral type (F25 and F35). No spectral features from the secondaries are apparent from comparison of our synthetic spectra to the observations, with the sole exception of the blue flank of the He I/N III 2.112-2.115 μm feature in F15 where unexpected emission is potentially present.

Stellar properties for these sources are presented in Table 2. The WNLh stars are found to be exceptionally luminous and support powerful stellar winds while, as expected, the O super-/hypergiants appear less luminous and drive lower density, higher velocity outflows. The carbon, nitrogen and oxygen abundances derived for all objects are consistent with equilibrium values for their respective evolutionary stages and no simultaneous enhancement of carbon and nitrogen - suggestive of binary interaction (cf. Clark et al. (2014)) - are observed. The only possible exception is F6, where carbon is less depleted; however this finding is consistent with the moderate He enrichment ($Y=0.33$). We highlight that our CNO estimates are consistent with an α -enhanced metallicity pattern for the Arches as also found by Najarro et al. ((2009)) in the Quintuplet cluster.

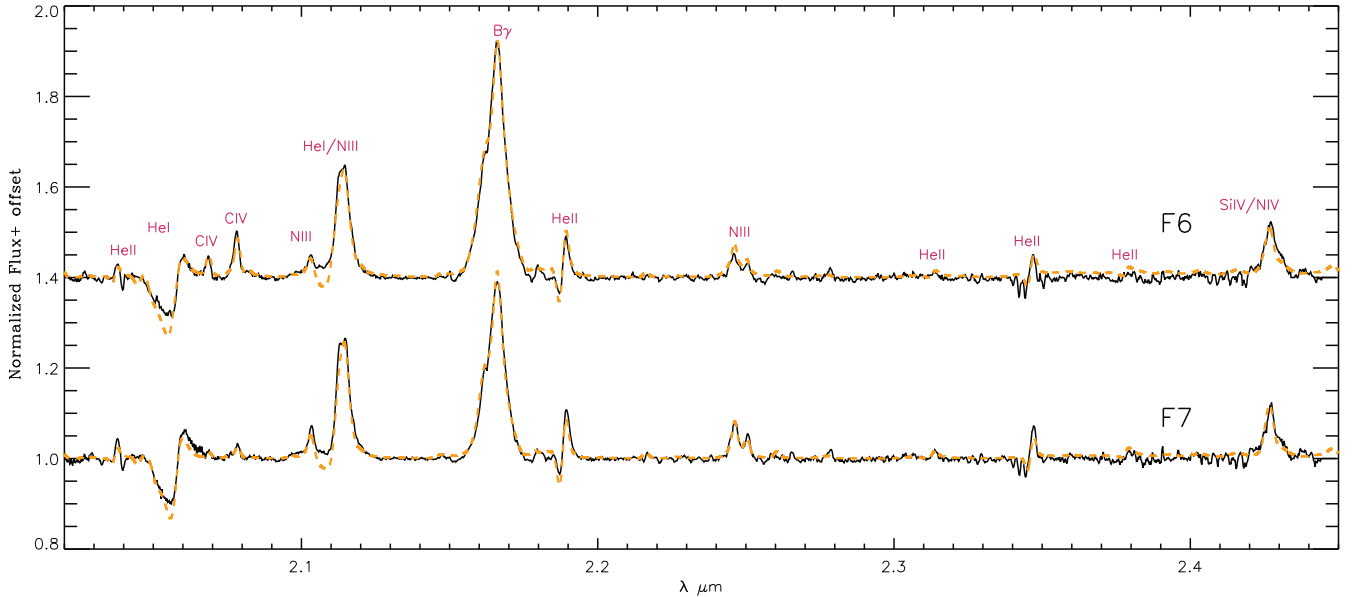
With the exception of F25, these stars were also analysed by Martins et al. ((2008)), while F15 had been previously modelled by Najarro et al. ((2004)). Both groups adopted a similar approach, with the main difference posed with the handling of extinction: Najarro et al. used a variable extinction description according to Moneti's law, while Martins et al. chose a fixed $A_K = 2.8$ value. We find very good agreement with the T_{eff} , L_* and v_∞ values from Martins et al. (their Table 2) for the WNLh stars F6 and F7; however, helium and carbon abundances for both stars are enhanced by, respectively, $\sim 50\%$ and $\sim 100\%$, while nitrogen in F6 demonstrates a $\sim 75\%$ enhancement with respect to this work. As for the O hypergiant, F15, our derived T_{eff} , L_* and helium abundances land in between the values provided by both studies and, while we find a consistent nitrogen abundance, our value for carbon is significantly higher than that of Martins et al., being driven by the difference in T_{eff} , and hence closer to the estimate of Najarro et al.

F35 demonstrates the largest discrepancy between both studies; where Martins et al. find $T_{\text{eff}}=33.5$ kK, we obtain $T_{\text{eff}}=40.0$ kK. We attribute this divergence to the weight given to the diagnostic He I/N III 2.112-2.115 μm feature. The absence of an observed ab-

Table 2. Best-fit stellar parameters for the arches RV systems from CMFGEN modelling and SED fitting.

Star	Spec. Type	A_{K_s}	T_{eff} kK	$\log(L_*)$ L_{\odot}^{-1}	R_* R_{\odot}	$\log(\dot{M})$ $M_{\odot} \text{ yr}^{-1}$	v_{∞} km s^{-1}	β	f_{cl}	Y	X_{N}	X_{C}	X_{O} mass fraction ($\times 10^{-3}$)
F6	WN8-9ha	3.01	33.3±1.3	6.32±0.05	43.4	-4.48±0.06	1400	1.10	0.10	0.33 $^{+0.08}_{-0.08}$	20	0.75	≤ 1.0
		3.63		6.57±0.05	50.0	-4.30±0.06							
		1.97		5.89±0.05	26.5	-4.81±0.06							
F7	WN8-9ha	3.01	33.9±1.3	6.27±0.05	39.7	-4.70±0.06	1250	1.05	0.08	0.45 $^{+0.08}_{-0.08}$	22	0.24	≤ 3.0
		3.59		6.52±0.05	52.7	-4.52±0.06							
		1.97		5.57±0.05	24.5	-5.01±0.06							
F15	O6-7 Ia ⁺	2.78	32.0±1.5	5.90±0.06	29.0	-5.33±0.08	2100	1.35	0.10	0.17 $^{+0.05}_{-0.03}$	6.6	2.0	11
		3.34		6.14±0.06	38.0	-5.16±0.08							
		1.82		5.51±0.06	18.4	-5.63±0.08							
F25	O4-5 Ia	3.81	40.0±2.0	5.93±0.06	19.1	-6.06±0.13	2200 ²	1.15	0.10	0.10 $^{+0.03}_{-0.02}$	5.5	5.3	14
		4.56		6.23±0.06	27.1	-5.83±0.13							
		2.52		5.51±0.06	18.4	-6.44±0.13							
F35	O4-5 Ia	2.80	40.0±2.0	5.77±0.07	16.0	-6.17±0.13	2200 ²	1.15	0.10	0.10 $^{+0.03}_{-0.02}$	4.8	7.8	14
		3.36		6.00±0.07	20.9	-6.00±0.13							
		1.85		5.38±0.07	10.2	-6.46±0.13							

Three different parameter sets are displayed as a function of the extinction law adopted: the uppermost is our favoured two α prescription, the middle a Moneti law and the latter a single α law (Sect. 4). T_{eff} and R_* correspond to ($\tau_{\text{Ross}} = 2/3$). f_{cl} and β are the clumping factor and velocity-law parameters as given in Najarro et al. ((2009)). Y is the He/H ratio by number and CNO abundances are provided as mass fractions. Uncertainties in the extinction law and distance (8 kpc) to the cluster are not considered. Therefore, L_* estimates only propagate errors in T_{eff} assuming a fixed observed flux in the Rayleigh-Jeans-like NIR bands (i.e. $\propto T_{\text{eff}} R_*^2$). Errors in the terminal velocities of F6 & F7 are $\approx 150 \text{ km s}^{-1}$ and $\approx 200 \text{ km s}^{-1}$ for F15 while a value of $v_{\infty} = 2200 \text{ km s}^{-1}$ has been assumed for the O-supergiants F25 and F35. Nitrogen abundance uncertainties are $\sim 0.15\text{dex}$ for the WNh stars and $\sim 0.20\text{dex}$ for the O stars, while we estimate a $\sim 0.30\text{dex}$ uncertainty in the Carbon abundance. Only upper limits could be set on the Oxygen abundance of F6 and F7 WNh stars, while a $\sim 0.30\text{dex}$ uncertainty is obtained for the O stars F15, F25 and F35.

**Figure 7.** Comparison of model fits (orange dotted lines) to observational spectra of WNLh primaries (black solid lines). Major spectral transitions are indicated.

sorption component points towards a higher T_{eff} (earlier type) than the one obtained by Martins et al.

4.2 Location in the HR diagram

Figure 9 shows the location of these systems in the HR diagram, together with non-rotating Geneva model and isochrones (Ekström et al. (2012)). We also show the position of both the individual compo-

nents of the SB2 binary F2 along with its integrated properties (Lohr et al. (2018)). Bearing in mind that both F6 and F7 appear dominated by their primaries, their near coincidence in the HR diagram with the WNLh primary of F2 endorses the independent results from the latter work.

From Fig. 9 we see that non-rotating models indicate initial masses of $\sim 100\text{--}120M_{\odot}$ for the WNh primaries of F2, F6, and F7. Values around $60M_{\odot}$ are suggested for the O stars, although the resultant

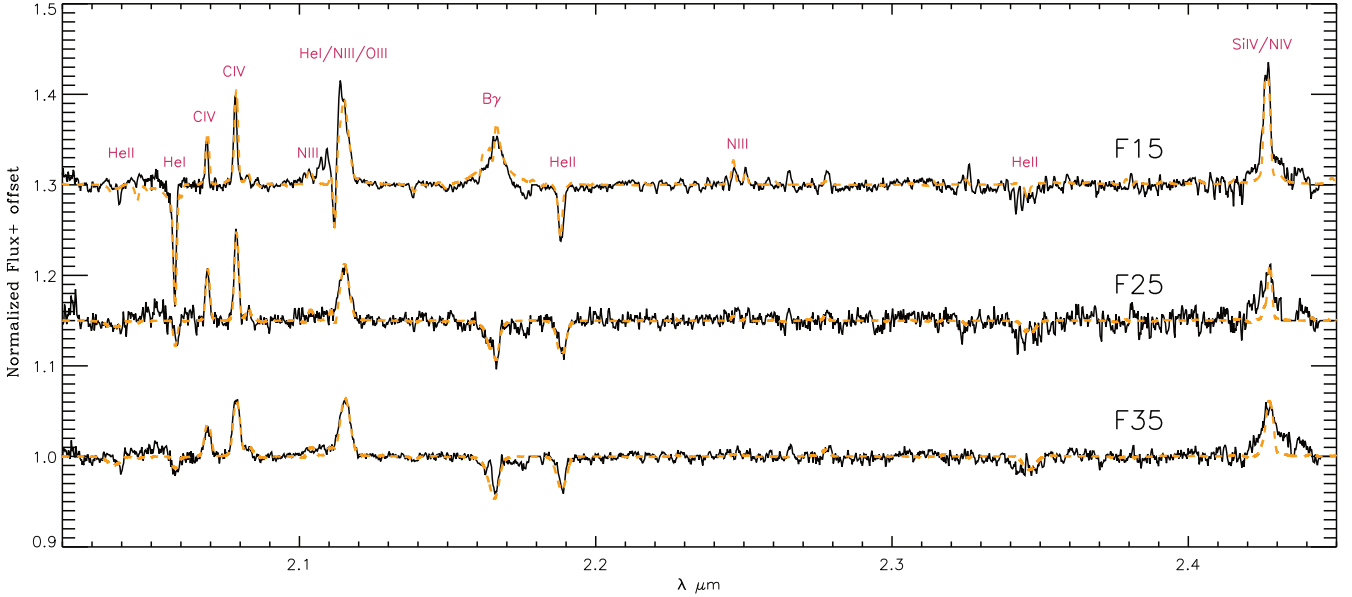


Figure 8. Comparison of model fits (orange dotted lines) to observational spectra of O super-/hypergiant primaries (black solid lines). Major spectral transitions are indicated.

mass range might extend downwards to $\sim 40 - 50M_{\odot}$ if the secondaries in the supergiant binaries F25 and F35 contribute significantly to their integrated fluxes. Taken in isolation these results should be treated with caution, as they display a critical dependence on the final extinction law assumed. However, in view of our analysis of the whole sample (Najarro et al. in prep.), we anticipate that they should be close to the final values. Moreover we highlight that initial masses ranging from $\sim 60-120M_{\odot}$ are fully consistent with the dynamical masses determined for the components of F2 (Table 3; Lohr et al. (2018)), buttressing the reliability of our evolutionary values.

Finally, the properties of F2, F6, F7, F25, and F35 are consistent with a cluster age of 2.0-2.5 Myr, as suggested by a number of studies (Figer et al. (2002), Najarro et al. (2004), Clark et al. (2018a) and is consistent with the results of Najarro et al. (in prep.). The location of F15 in the HR diagram suggests a slightly larger age of ~ 2.8 Myr, although it is still consistent with the range defined by the former stars upon consideration of the relevant observational and modelling uncertainties.

5 DISCUSSION

The synthesis of multi-wavelength observational data and quantitative model atmosphere analysis reveals that the Arches cluster is characterised by a rich population of very massive binaries. Previous spectroscopic binary surveys have targeted field stars (e.g. Mason et al. (2009), Chini et al. (2012), Sota et al. (2014)), a number of comparatively low mass clusters (Sana et al. (2012)) and large stellar aggregates such as the Cyg OB2 association (e.g. Kobulnicky et al. (2014)) and 30 Doradus (Sana et al. (2013a), Dunstall et al. (2015), Almeida et al. (2017)). While these studies provide a significantly larger sample size than that furnished by the Arches, the stars considered are heterogeneous in terms of age and hence evolutionary phase. While the cohort derived from Westerlund 1 is thought to be co-eval (Ritchie et al. (2009), Clark et al. (2020)) it is older than the Arches, and hence samples lower mass OB and WR stars. Indeed,

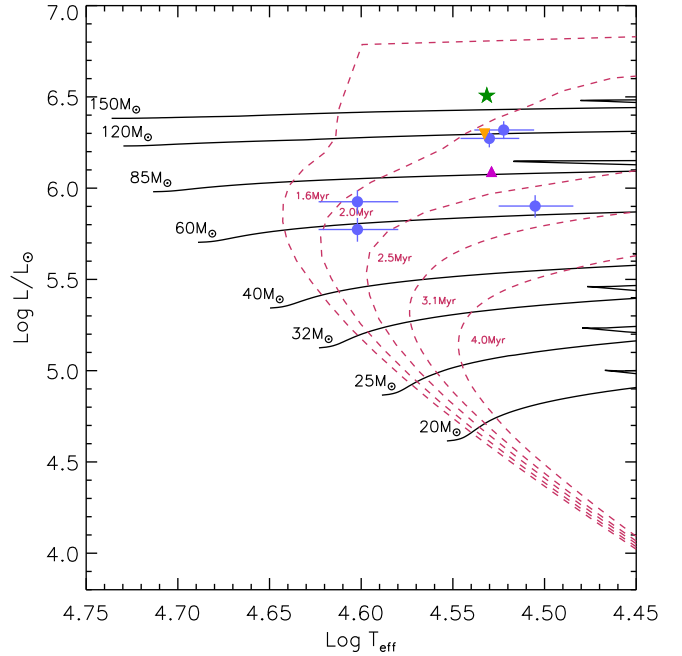


Figure 9. HR diagram displaying the RV arches objects together with non-rotating Geneva model and isochrones. Stellar luminosities are those from the two- α extinction fits in Table 2. We also plot the position of the SB2 binary F2 (green-star) as well as the locations of the WN9h primary and O5-6 Ia⁺ secondary components (yellow and purple triangles respectively) from the unconstrained binary modelling by Lohr et al. ((2018)).

with the exception of 30 Dor, none of these surveys reach a comparably rich contingent of very massive stars. As a consequence the Arches currently provides a unique (and complementary) perspective on the properties of such objects.

Critically, we find that Arches members exhibit a remarkably high

binary fraction: $\geq 50\%$ for $M \geq 60M_{\odot}$, rising to $\geq 62\%$ if only the more massive and evolved WNLh subset are considered. Although we consider the parameters for the binaries considered in Sect. 3 to be provisional, and contingent on future observations, it appears likely that a number have (highly) eccentric orbits - F2, F6, F25, and F35 (Table 1) - indicative of a pre-interaction evolutionary phase. Likewise, an orbital period apparently in excess of 3 years would appear to exclude prior interplay between the components of F7, although we cannot reject the possibility that the primary is itself a merger remnant. Crucially however, with periods $< 14d$, the compact nature of both F2 and F6 likely precludes such a scenario. As such, we are left to conclude that their components are not the product of mass transfer or merger, although the short orbital periods of many of the Arches binaries imply that future binary interaction is unavoidable (Sect. 3 and Table 3). Such a conclusion is at least consistent with the homogeneity of the spectra of the most massive stars within the Arches (Clark et al. (2018a)), although we caution that it is possible that putative blue stragglers might not differ significantly in terms of spectral morphology from less massive stars in the upper reaches of the HR diagram.

Schneider et al. (2014) argued that the most massive 9 ± 3 stars in the Arches cluster are the rejuvenated products of binary interactions. The conclusions outlined above appear at odds with this result. As discussed in Paper II, one explanation for this discrepancy is that Schneider et al. (2014) assumed an age of 3.5 Myr for the Arches cluster, which now appears to be at the upper end of the age range based on the age inferred from spectroscopic analyses (e.g. Papers I, II) and the results presented here (which both favour ages in the range 2-2.5 Myr). Assuming an age of 2.5 Myr, a cluster mass of $1.5 \times 10^4 M_{\odot}$ (Clarkson et al. (2012)) and an initial binary fraction of 100%, interpolating Fig. 5 of Schneider et al. (2014) would result in roughly an average of roughly 2 ± 3 of the most massive stars being the result of rejuvenated binary interaction in the Arches cluster.

Based on the above, we suggest that the current most massive stars in the Arches cluster may not be the products of binary mass-transfer or mergers of lower mass stars. That makes the Arches cluster, and these stars, crucial indicators of single stellar evolutionary models in the $> 50 M_{\odot}$ regime and highlights the urgency of follow-up observations to better characterise their orbital properties and better establish their evolutionary histories.

5.1 Spectral variability

With the first high S/N and resolution spectra of members of the Arches obtained in 1999 (Figer et al. (2002)), a second epoch in 2005 (Martins et al. (2008)) and extensive monitoring between 2011-2018 (Table A1), an observational baseline of ~ 2 decades permits a search for the characteristic long term spectral variability. To our knowledge, this is the first study that permits the assessment of long term variability in WNLh/O Ia⁺ stars. Despite such a baseline, none of the 37 targets display any evidence of spectral variability given our S/N and resolution limitations, as might be expected if the WNLh/O Ia⁺ cohort were close to the S Doradus instability strip. In Appendix B, we discuss the implications of the lack of spectral variability observed in the current sample, with respect to the secular variability observed in LBVs. This seems unlikely to be the result of observational limitations given the variability exhibited in the LBV spectra of the Quintuplet cluster (Clark et al. (2018b) and references therein).

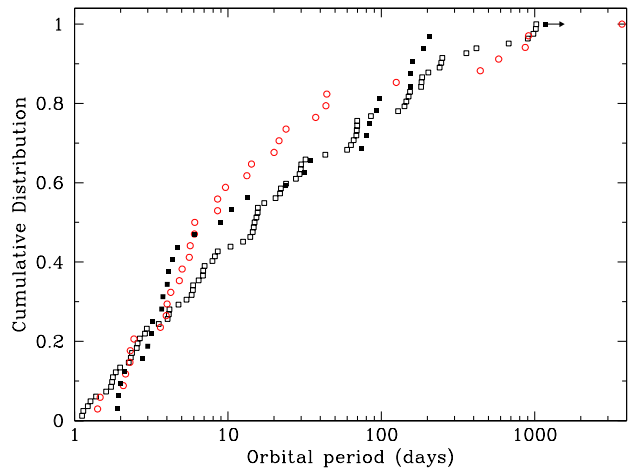


Figure 10. Plot of the cumulative distributions of orbital periods from the sample of WNLh and O super-/hypergiants given in Table 3 (filled squares), O stars in Galactic clusters (red circles; Sana et al. (2012)) and in 30 Dor (open squares; Almeida et al. (2017)). Given their uncertain periods, RMC136c and F25 are excluded from this plot, while the value for F7 is a lower limit.

5.2 The Arches population in context: fundamental properties of WNLh stars and O hypergiants

It is instructive to place the properties of the binary population of the Arches into a wider context. In Table 3 we summarise the orbital properties of other WNLh (and the related Of/WN stars) and O hypergiants within the Galaxy and Large Magellanic Cloud (noting that a lack of comparator systems prevents extending this exercise to the cluster mid-O supergiants), while in Appendix C we compare the properties of the subset of WNLh stars found within stellar aggregates. In doing so we note that slightly earlier subtypes are present within R136/30 Doradus (WN5-6ha and O2-2.5 If/WN5-6) and some Milky Way clusters (e.g the WN6ha stars within NGC3603); it is not clear whether this disparity results from different initial masses, ages or metallicities, or a combination of these properties.

5.2.1 Masses and evolutionary state

Consideration of the dynamical masses listed in Table 3 supplemented, where available, by evolutionary masses determined from quantitative modelling (cf. Table C1) confirm the conclusions derived from the Arches population: that the WNLh stars and mid-O hypergiants appear to form a homogenous class of uniquely massive objects. Masses range from $\sim 50M_{\odot}$ (WR29 and RMC145; Table 3) to $\gg 100M_{\odot}$ (the WN5ha components of R136; Crowther et al. (2016)) for the former, with the latter potentially being somewhat lower (Table 3)⁹. Their masses therefore exceed those of O dwarfs (Clark et al. (2018a)), consistent with the suggestion that they are relatively unevolved core-H burning stars populating the upper reaches of the stellar mass function, whose proximity to the Eddington limit leads to inflated envelopes and the development of powerful stellar

⁹ The high velocity runaway WR148 may be an exception to this conclusion (Table 3), although its dynamical mass determination is based on an assumed mass for the O secondary and, moreover, is dependent on the uncertain inclination of the system (Munoz et al. (2017)). Conversely, WR79a, the star with the lowest bolometric luminosity (Table C1) has an evolutionary mass of $\sim 60M_{\odot}$.

winds (Hamann et al. (2006), Schnurr et al. (2009a), Crowther et al. (2010), Gräfener et al. (2021)). This interpretation is buttressed by the analysis of Hamann et al. ((2019)) who show that the most luminous WN stars are exclusively WNL stars with pronounced signatures of hydrogen in their spectra.

Such conclusions are consistent with the observational finding that WNLh stars appear confined to the youngest coeval clusters within both galaxies ($< 4\text{Myr}$; Appendix C and refs. therein), being present within Mercer 30 ($4.0^{+0.8}_{-0.8}\text{Myr}$; de la Fuente et al. (2016)) and Mercer 81 ($3.7^{+0.4}_{-0.5}\text{Myr}$; Davies et al. (2012a)) and seen in relative profusion in still younger clusters such as R136 ($1.5^{+0.3}_{-0.7}\text{Myr}$; de Koter et al. (1998); Crowther et al. (2016)), but absent from the slightly older Westerlund 1 ($\sim 5 - 6\text{Myr}$; Negueruela et al. (2010), Clark et al. (2020)).

In this regard we highlight that WR121a (WN7ha) is found in the core of the deeply embedded cluster within the Giant H II region W43 (Blum et al. (1999)), while MMT58 (O2-3.5 If*/WN5-6ha) is located within a compact H II region on the periphery of the star-forming region surrounding NGC3603 (Roman-Lopes (2013)). Their environments suggest extreme youth for both stars - with Roman-Lopes ((2013)) estimating a dynamical age of $< 600, 000\text{yr}$ for the latter system - allowing limited opportunity for the prior interaction of the binary components of both systems. Furthermore both stars are found to be in very compact configurations ($P_{\text{orb}} \lesssim 4\text{d}$; Table 3) which would appear to disfavour their formation via prior mergers (cf. Arches F2 and F6). As a consequence we conclude that such very massive stars are able to form monolithically, without requiring binary mass transfer or merger on or after the main sequence to attain their final masses, a hypothesis also suggested by the properties of the Arches binary cohort. Nevertheless, it is clear that a subset may also form via a binary channel, as evidenced by the presence of the highly (over)luminous mid-O hypergiant blue stragglers Wd1-27 (O7-8 Ia⁺) and Wd1-30a (O4-5 Ia⁺) within Westerlund 1 (Clark et al. (2019a)).

5.2.2 Binary properties and frequency of occurrence

We now turn to the physical properties of the subset of the WNLh and O hypergiant population for which binary solutions have been obtained (Table 3). In doing so we are conscious of the observational biases introduced by the differing sensitivities, durations and cadences of the observations used in both the construction of this sample, and in comparison to the wider surveys of lower mass stars mentioned above. Accounting for this would require Monte Carlo simulations for every individual study in order to quantify their completeness as a function of orbital parameters, beyond the scope of the work.

Mindful of this, we first turn to orbital separation and in Fig. 10 we plot the cumulative distribution of orbital periods for the stars listed in Table 3, alongside the population of Galactic O stars of Sana et al. ((2012)) and the corresponding cohort in 30 Dor (Almeida et al. (2017)). We note that the latter two distributions are constructed for stars that, on average, are expected to be of lower mass than those considered here; dynamical and evolutionary mass estimates suggest $M \lesssim 47M_{\odot}$ for the 30 Dor sample (Mahy et al. (2020a), (2020b)), while that of Sana et al. ((2012)) is predominantly populated by late O dwarfs and giants of moderate luminosity. Furthermore, in undertaking this comparison we explicitly highlight that, as with the latter authors, we have not applied any bias corrections to these data. As a consequence detailed quantitative analysis is premature but, following the argument of Almeida et al. ((2017)) that one might expect

differing studies to suffer similar biases, a qualitative comparison is potentially instructive.

The three cumulative distributions look to be broadly similar. To the naked eye, the one constructed for WNLh stars and O hypergiants and that derived for Galactic O stars by Sana et al. ((2012)) show a close correspondence, appearing to be overabundant in binaries with $P_{\text{orb}} \sim 4 - 40\text{d}$ with respect to that of Almeida et al. ((2017)) for O stars within 30 Dor; however these authors show that there are no statistically significant differences between these distributions. As might be expected we identify a predominance of comparatively short orbital period systems, with $\sim 50\%$ of binaries listed in Table 3 found with periods of less than a week, $\sim 70\%$ less than a month and $\sim 97\%$ less than a year (the ratios being identical if just the subset of WNLha stars are considered). These numbers appear comparable to the findings of Almeida et al. ((2017)) and Sana et al. ((2012)), who report percentages of 40%, 70% and 90%; and 50%, 74% and 85% for these period intervals for, respectively, O-star binaries within 30 Dor and Galactic clusters.

Evidently, the distributions are in part representative of the observing strategies employed, which disfavour the characterisation of binaries with multi-year periods (cf. F7; Sect. 3). Conversely, while the identification of short period systems appears favoured, such very massive and compact binaries still have to exist in order to be detected. In this regard we highlight that the shortest period binaries within the WNLha sample are the $P_{\text{orb}} \sim 1.9\text{d}$ systems BAT99-32 and MMT58; in contrast the 30 Dor O star sample hosts 10/82 binaries with shorter orbital periods than this, with a minimum $P_{\text{orb}} \sim 1.1\text{d}$ (VFTS066 and 352). One could attribute this apparent discrepancy to binary interaction/merger amongst the WNLh cohort, but we note that the short period 30 Dor O star binaries are exclusively of luminosity class III-V; consequently an alternative (or complementary) explanation would be that the larger radii of the WNLh stars prohibits the formation of such tight binaries. Indeed, by way of an illustration, quantitative estimates of the stellar radii and masses of the components of Arches F2 (Lohr et al. (2018)) and WR20a (Rauw et al. (2005)) preclude the component stars being found in similarly compact configurations.

Sana et al. ((2012)) conclude that the rich population of comparatively short period binaries implies that fully 70% of the O stars they consider will interact at some point in their life cycle. Despite the similarity in orbital period distributions, uncertainties in the evolution of massive ($\gtrsim 60M_{\odot}$) stars - due to significant mass loss driven by stellar winds and instabilities - mean that this quantitative prediction is not immediately applicable to the sample considered here. However, if such stars pass through a comparatively ‘cool’, physically extended LBV-like phase (cf. the evolutionary predictions for a $M_{\text{initial}} \sim 60M_{\odot}$ star by Groh et al. (2014)) then one would also expect a large proportion will undergo binary interaction.

Moving on to orbital eccentricity, only a subset of WNLha and O super/hypergiants have observational determinations, but the proportion with essentially circular orbits ($e < 0.1$) appears broadly comparable to that of the 30 Dor O star sample (48% versus 40% respectively; Almeida et al. (2017)). Once again this is potentially explicable by a combination of tidal interaction and/or mass transfer, plus the inability for short period highly eccentric configurations to accommodate such physically massive stars.

Explicitly excluding the post-supernova X-ray binary HD153919, of those systems for which (lower limits to) dynamical mass estimates are available, it is apparent that the secondaries are also highly luminous stars; such a preponderance of massive companions is also seen in both 30 Dor (Almeida et al. (2017)) and Westerlund 1 (Clark et al. (2020); Ritchie et al. (2021)). This is likely to be in part an

observational bias; in order for mass determinations to be made one requires SB2 systems. As a consequence the companion has to be of comparable luminosity - and hence mass - to the primary in order to fulfil this requirement. Nevertheless, a number count of 14/33 SB2 systems appears difficult to explain with a mass distribution for the companion stars deriving from random sampling of a canonical IMF.

Finally we turn to the binary frequency for WNLh stars. In order to assess this we adopt a different approach - mirroring that of Sana et al. ((2012)) - and limit ourselves to a sample derived from examples within stellar clusters. This has four advantages: (i) mindful of the discussion in Sana et al. ((2013a)), it limits the potential bias towards the detection of (overluminous) binaries in a magnitude limited sample; (ii) given the chosen clusters are well studied the resultant populations are better defined inasmuch as we are complete for such stars; (iii) in many cases the cluster properties (distance and age) have been determined, allowing quantitative determination of stellar properties; (iv) a number of clusters have been subject to radio and X-ray observations, which provide additional binary diagnostics. Unfortunately, however, a lack of data precludes analysis of analogues of the Arches mid-O super-/hypergiants via such a methodology.

A detailed breakdown of properties of this population is provided in Appendix C, where we consider 11 Galactic clusters (excluding the Arches) as well as R136 and the 30 Dor star-forming region within the Large Magellanic Cloud. This yields a total of 21 WNLh (and related objects) within R136 and 30 Dor and 24 within the Galactic clusters, for which one or more observational diagnostics for binarity are available. As with the Arches we give primacy to RV survey data, though also employ extant radio and X-ray data to identify colliding wind systems; in order to achieve this goal we also provide a thorough reappraisal of the X-ray properties of single and binary WNLh stars (Appendix C). Despite our best efforts we consider the resultant counts to be conservative lower limits; this is due to the aforementioned limitations of RV surveys and the fact that some stars have not been subject to such efforts, with an assessment of binarity instead relying solely on radio and/or X-ray data. Nevertheless, we find binary fractions of 10/21 ($\sim 48\%$) for examples within R136 and 30 Dor and 15/24 ($\sim 63\%$) for Galactic clusters, both of which compare favourably to our estimate for the Arches (8/13 ($\sim 62\%$); Sect. 3). In total this suggests a minimum binary fraction of 33/58 ($\sim 57\%$) for WNLh stars which, following the preceding discussion, appear to comprise objects with $M_{\text{init}} \gtrsim 50M_{\odot}$.

Because of the different observational approaches adopted across various studies - and in particular the heterogeneous nature of the dataset constructed here - direct, quantitative comparison of the binary frequencies returned is potentially misleading. Nevertheless, previously published surveys suggest a landscape in which binarity is pervasive amongst OB stars. Allowing for biases in their RV dataset, Kobulnicky et al. ((2014)) infer a fraction of $\sim 55\%$ for OB binaries with $P_{\text{orb}} < 5000\text{d}$ within the Cygnus OB2 association, Sana et al. ((2012)) return $\sim 69 \pm 9\%$ for O stars within a subset of Galactic clusters, and Sana et al. ((2013a)) quote $\sim 54 \pm 4\%$ for O stars within 30 Doradus. Our results appear fully consistent with such a picture and extend the predominance of binarity to the most massive stars in the local Universe.

6 CONCLUDING REMARKS AND FUTURE PROSPECTS

In this paper we have presented the results of a long term spectroscopic monitoring campaign of the massive members of the Arches cluster. With the inclusion of previous published data the baseline of observations extends to $\sim 19\text{yrs}$ yet no stars show evidence for long

term secular variability, such as that seen in LBVs. This is surprising since both observational data and theoretical simulations suggest that comparably massive stars should encounter this evolutionary phase (Appendix B). Nevertheless, this lack of variability permits the primary science goal of the programme - an assessment of the binary frequency and properties of very massive stars. We find 13 RV variables from a total of 37 stars ($\sim 35\%$), which rises to $\sim 60\%$ if the RV threshold is relaxed slightly; of these, provisional orbital solutions are reported for five stars and constraints for a further two. Orbital periods range from $\sim 6\text{d}$ to $\gtrsim 1184\text{d}$, with a number showing pronounced eccentricity (Sect. 3.1).

Examination of X-ray and radio data in order to identify the radiative signature of colliding wind systems identifies three additional candidate binaries, while the composite thermal+non-thermal radio spectra of a further three are at least consistent with binarity (Sect. 3.2). Excluding the latter stars at this time - and prior to correction for observational biases - we report a conservative lower limit to the cluster binary fraction of 16/37 ($\sim 43\%$). However we are both incomplete for the O supergiant cohort and less sensitive to variability in these stars by virtue of their lower S/N spectra, so a fraction of 10/20 for the combined - and completely sampled - WNLh and O hypergiant populations is more instructive (rising to 8/13 for the former stars alone; Sect. 3.3).

Dynamical mass estimates for the sole eclipsing SB2 binary F2 suggest extreme current masses for both WN8-9ha ($82 \pm 12M_{\odot}$) and O5-6 Ia+ ($60 \pm 8M_{\odot}$) components. Quantitative model atmosphere analysis for the remaining binary candidates subject to orbital analysis is consonant with this finding, allowing us to infer evolutionary initial masses of $\sim 100-120M_{\odot}$ for the WNLh stars and $\gtrsim 60M_{\odot}$ for the O stars. Both findings are consistent with an age of $\sim 2.0-2.5\text{Myr}$ for the Arches.

Several conclusions follow directly from consideration of these data. The combination of short orbital periods and significant eccentricities of F6 and F35 strongly suggests that they are pre-interaction systems (Table 3); as a consequence it would appear that the very massive stars within the Arches do not form exclusively via binary mass transfer and/or merger of lower mass stars (cf. Schneider et al. (2014)). Indeed we find no evidence for ongoing or recent binary interaction amongst any cluster members (Clark et al. (2018a)), although we cannot exclude the possibility that a subset of stars are the product of such an evolutionary channel. Secondly, star formation in the extreme conditions prevalent in the CMZ yields very massive (binary) stars in a similar manner to more quiescent regions of the Galaxy. This is of particular interest since the environment of the CMZ is thought to closely resemble that of high-redshift star-forming galaxies (Kruijssen & Longmore (2013)), suggesting that star formation may proceed in a comparable manner in such objects.

The properties of the Arches members are better understood by being placed in a wider context, and we provide a summary of the properties of all known WNLha and O-type hypergiant binaries in Table 3. This enlarged dataset shows that such stars are exceptionally massive, with dynamical and evolutionary mass determinations suggesting a lower limit of $\sim 50M_{\odot}$, with extreme examples greatly exceeding $100M_{\odot}$. We highlight that such a mass range is in excess of that sampled in previous studies of OB binaries (Sana et al. (2012), Kobulnicky et al. (2014), Almeida et al. (2017)). Nevertheless, within observational uncertainties and before correction for survey biases, we find no evidence that the physical properties of the WNLh and O hypergiant binaries - orbital period, eccentricity and mass ratio distributions - significantly differ from those of lower mass OB stars. The sole exception to this is an apparent absence of WNLh and O hypergiant binaries with very short orbital periods ($\lesssim 1.9\text{d}$), poten-

Table 3. Published parameters for binaries with WNLha and mid-O super-/hypergiant primaries, ordered by increasing orbital period

Name	Spectral types	P_{orb} (d)	e	$M_1 + M_2$ (M_{\odot})	Aggregate	References
BAT99-32	WN6(h) + ?	1.91	0.0	-	-	(1)
MMT58	O2-3.5 If*/WN5-6ha + ?	1.936	0.0 (assumed)	84.5 + 31	NGC3603	(2)
BAT99-6	O3If*/WN7 +OB +SB1	2.0	0.0	-	-	(3)
RMC135	WN7h + ?	2.112	0.0 (assumed)	-	30 Dor	(1)
RMC140b	WN5h + O	2.76	0.23	-	30 Dor	(1)
BAT99-77	WN7ha + ?	3.00	0.32	-	-	(1)
WR29	O + WN7h	3.164	0.0 (assumed)	53.3±3.5 + 42.1±3.5	-	(4,5)
BAT99-12	O3If*/WN6 + ?	3.23	0.34	-	-	(1)
WR20a	WN6ha + WN6ha	3.7	0.0	83±5 + 82±5	Wd2	(6,7,8)
NGC3603-A1	WN6ha + WN6ha	3.77	0.0	116±31 + 89±16	NGC3603	(9,10)
WR121a	WN7ha + ?	4.1	0.0 (assumed)	-	W43	(11)
WR148	WN7ha + O5V	4.32	0.0	(33±37)	-	(12)
Mk30	O3If*/WN6 + ?	4.70	0.20	-	30 Dor	(1)
RMC136c	WN5h + ?	~ 8.4	0.0 (assumed)	-	30 Dor	(13)
NGC3603-C	WN6ha + ?	8.89	0.30	-	NGC3603	(9,10)
F2	WN8-9h + O5-6 Ia ⁺	10.5	0.075	82±12 + 60±8	Arches	(14)
F6	WN8-9h + ?	13.378	0.6	-	Arches	(this work)
WR12	WN8h + ?	23.9	0.0	-	-	(15)
WR21a	O3/WN5ha + O3Vz((f*))	31.672	0.695	64.4±4.8 + 36.3±1.7 (103.6±10.2 + 58.3±3.7)	-	(16,17,18)
RMC144	WN6h + WN6h	70.4	0.51	> 48.6 ± 1.8 + > 45.7 ± 1.9 (74 ± 4 + 69 ± 4)	30 Dor	(19)
WR22	WN7+abs + O9	80.3	0.598	> 55.3 ± 7.3 + > 20.6 ± 1.7	Carina	(20,21,22)
Mk37	O2.5If*/WN6 + ?	92.6	0.0 (assumed)	-	30 Dor	(1)
Mk34	WN5h + WN5h	155.1	0.68	> 65 ± 7 + > 60 ± 7 (139 ⁺²¹ ₋₁₈ + 127 ⁺¹⁷ ₋₁₇)	30 Dor	(23)
RMC145	WN6h + O3.5 If*/WN7	159	0.78	53 ⁺⁴⁰ ₋₂₀ + 54 ⁺⁴⁰ ₋₂₀	30 Dor	(24,25)
J1745-28	WN9h + ?	189	-	-	-	(26,27)
WR25	O2.5If*/WN6 + O	207.7	0.56	75±7 + 27±3	Carina	(28,29)
F7	WN8-9h + ?	≥1184.46	-	-	Arches	(this work)
HD153919	O6.5Iaf ⁺ + cc	3.412	0.0 (assumed)	58 ⁺¹¹ ₋₁₁ + 2.44 ^{+0.27} _{-0.27}	-	(30)
Cyg OB2 B17	O7Iaf + O9Iaf	4.022	0.0 (assumed)	60 ⁺⁵ ₋₅ + 45 ⁺⁴ ₋₄	Cyg OB2	(31)
F25	O4-5 Ia + ?	~ 5 - 9?	> 0.0	-	Arches	(this work)
F35	O4-5 Ia + ?	6.043	0.44	-	Arches	(this work)
HD166734	O7If + O9If(f)	34.5	0.618	39.5 ^{+5.4} _{-4.4} + 33.5 ^{+4.6} _{-3.7}	-	(32)
F15	O6-7 Ia ⁺ + ?	83.95	0.0	-	Arches	(this work)
LS III+46 11	O3.5If* + O3.5 If*	97.2	0.56	> 38.8 ± 0.8 + > 35.6 ± 0.8	Berkeley 90	(33)
RMC139	O6.5Iafc + O6Iaf	153.9	0.382	> 69.4 ± 4.1 + > 53.9 ± 3.1	30 Dor	(34,35)

Component masses given in parenthesis for WR21a and WR148 are determined under the expectation of a canonical mass for the O3Vz and O5V secondaries (Tramper et al. (2016), Munoz et al. (2017)), while those for Mk34 are inferred from spectroscopic analysis (Tehrani et al. (2019)). References used in the construction of this table are: (1) Schnurr et al. ((2008b)); (2) Jaque Arancibia et al. ((2015)); (3) Niemela et al. ((2001)); (4) Niemela & Gamen ((2000)); (5) Gamen et al. ((2009)); (6) Rauw et al. ((2004)); (7) Bonanos et al. ((2004)); (8) Naze et al. (2008); (9) Moffat et al. ((2004)); (10) Schnurr et al. ((2008b)); (11) Arora & Pandey ((2020)); (12) Munoz et al. ((2017)); (13) Schnurr et al. ((2009b)); (14) Lohr et al. ((2018)); (15) Fahed & Moffat ((2012)); (16) Benaglia et al. ((2005)); (17) Niemela et al. ((2008)); (18) Tramper et al. ((2016)); (19) Shenar et al. ((2021)); (20) Rauw et al. ((1996)); (21) Schweickhardt et al. ((1999)); (22) Gräfenor & Hamann ((2008)); (23) Tehrani et al. ((2019)); (24) Schnurr et al. ((2009a)); (25) Shenar et al. ((2017)); (26) Mikles et al. ((2008)); (27) Clark et al. ((2009)); (29) Gamen et al. ((2008)); (29) Hur et al. ((2012)); (30) Clark et al. ((2002)); (31) Stroud et al. ((2010)); (32) Mahy et al. ((2017)); (33) Maíz Apellániz et al. ((2015)); (34) Taylor et al. ((2011)); (35) Mahy et al. ((2020a))

tially due to a combination of binary evolution depleting the tightest systems, and their physical extent, which precludes their accommodation within such compact configurations. As with the Arches, the pronounced eccentricities of a number of short period systems suggests they are in a pre-interaction state. In this regard the compact binaries MMT58 and WR121a are of particular interest due to the extreme youth implied for them as a result of their location within active star forming regions (Sect. 5.1). Taken as a whole these ob-

servations bolster the conclusion from the Arches cohort that very massive WNLh stars do not solely form via a binary channel.

In order to assess the frequency of occurrence of binarity amongst WNLh stars we followed the approach of Sana et al. ((2012)) and reviewed the properties of those found in stellar clusters utilising a combination of radial velocity, radio and X-ray data. This required a re-analysis of extant X-ray data. This revealed that while single WNLh stars appear to be intrinsically faint, binaries hosting them

appear to be amongst the most luminous of all non-accreting stellar systems, with $\sim 76\%$ confirmed examples lying above a $(L_x/L_{\text{bol}}) \sim 10^{-7}$ threshold; we consequently adopt this as an identifier for CWBs.

Utilising all diagnostics at our disposal we identify a total of 33/58 binaries amongst the complete sample, noting that is almost certainly a lower limit to the true frequency given the limitations of the datasets utilised (Sect. 4 and Appendix C). Because of different observational approaches adopted, quantitative comparison of this value to the binary frequencies returned by other surveys is potentially misleading. Nevertheless, even before correcting for bias and incompleteness our results appear qualitatively consistent with the hypothesis that the high binary fraction of very massive ($> 50M_{\odot}$) stars continues the trend found for lower mass OB stars by other large scale surveys (Sect. 5.1.2).

Such a finding has important implications for a number of diverse astrophysical questions including implications for the birth of very massive stars in extreme environments, which has already been discussed, the inference of the (DMF from an observational luminosity function (cf. Schneider et al. (2014)), and at larger scales, there is an increasing realisation that such extremely luminous stars play a substantive role in (i) the provision of ionising, radiative feedback (e.g. Doran et al. (2013)) and (ii) the production of cosmic rays and subsequently high energy (TeV) γ -ray emission via particle acceleration in wind shocks.

In order to fully address these questions it is clear that we will have to expand and refine our current dataset to better understand the impact of binarity on the formation, evolution and fate of WNh stars. In terms of the Arches this will necessitate (i) Monte Carlo simulations to account for biases introduced by differences in the cadence and number of observations of individual stars, (ii) the population of a cluster HR diagram via model atmosphere analysis in order to place the binaries into context, and (iii) an increased observational effort to derive orbital solutions for the full cohort of RV variables. Expanding this undertaking to include Mercer 30 & 81, Danks 1, HM-1, Sco OB2 and W43 would raise the sample size exposed to multi-epoch spectroscopic observations by 15, with a further 12 unstudied examples distributed through the CMZ (Clark et al. (2021)) and seven additional targets within the outskirts of Wd2, NGC3603 and 30 Dor. Although observationally expensive, such an effort would increase the number of WNh stars subject to such investigations to 77, effectively doubling the sample size. Assuming an empirical binary fraction of $\geq 60\%$, this would allow the determination of the full suite of orbital parameters for a statistically robust sample of ≥ 50 binaries containing the most massive stars currently forming within the local Universe. We note that confirmation of the frequency of occurrence would also be a central outcome of such a programme.

ACKNOWLEDGEMENTS

We thank the referee, Alex de Koter, for providing a thorough review with helpful comments and interesting arguments. F.N. acknowledges funding by grants PID2019-105552RB-C41 and MDM-2017-0737-19-3 Unidad de Excelencia "María de Maeztu". LRP acknowledges the support of the Generalitat Valenciana through the grant APOSTD/2020/247. This research is partially supported by the Spanish Government under grant PGC2018-093741-B-C21 (MICIU/AEI/FEDER, UE).

DATA AVAILABILITY

Table 1 contains the results of the radial velocity analysis and is available via the CDS service. The individual radial velocity measurements for each epoch for all targets are available in Table A1 and is available as supplementary material (online). Appendix C1 contains the details of how the X-ray observations were compiled and is available as supplementary material (online). The raw spectroscopic observational data can be freely obtained from the ESO Science Archive Facility.

REFERENCES

- Almeida, L. A., Sana, H., Taylor, W. et al. 2017, *A&A*, 598, A84
 Antokhin, I. Bertrand, J.-F., Lamontagne, R., Moffat, A.F. J., & Matthews, J. 1995, *AJ*, 109, 817
 Arora, B. & Pandey, J. C. 2020, *ApJ*, 891, 104
 Belczynski, K., Kalogera, V., Radio, F. A., et al. 2008, *ApJS*, 174, 223
 Benaglia, P., Romero, G. E., Koribalski, B. & Pollock, A. M. T. 2005, *A&A*, 440, 743
 Bestenlehner, J. M., Vink, J. S., Graefener, G. et al. 2011, *A&A*, 530, L14
 Blum, R. D., Daminieli, A., & Conti, P. S. 1999, *AJ*, 117, 1392
 Blum, R. D., Schaefer, D., Pasquali, A. et al. 2001, *AJ*, 122, 1875
 Bonanos, A. Z. Stanek, K. Z., Udalski, A. et al. 2004, *ApJ*, 611, L33
 Bonnet, H., Abuter, R., Bkaer, A. et al. 2004, *Messenger*, 117, 17
 Borissova, J., Georgiev, L., Hanson, M. M., et al. 2012, *A&A*, 546, A110
 Cappa, C., Goss, W. M. & van der Bucht, K. A. *AJ*, 127, 2885
 Chapman, J. M., Leitherer, C., Koribalski, B., Bouter, R. & Storey, M. 1999, *ApJ*, 518, 890
 Chené, A.-N., Borissova, J., Bonatto, C., et al. 2013, *A&A*, 549, A98
 Chené, A.-N., Ramírez Alegría, Borissova, J. et al. 2015, *A&A*, 584, A31
 Chini, R., Hoffmeister, V. H., Nasseri, A., Stahl, O. & Zinnecker, H. 2012, *MNRAS*, 424, 1925
 Clark, J. S., Goodwin, S. P., Crowther, P. A., et al. 2002, *A&A*, 392, 909
 Clark, J. S., Crowther, P. A. & Mikles, V. J. 2009, *A&A*, 507, 1567
 Clark, J. S., Ritchie, B. W., Negueruela, I., 2010, *A&A*, 514, A87
 Clark, J. S., Castro, N., Garcia, M. et al. 2012, *A&A*, 541, A146
 Clark, J. S., Ritchie, B. W., Najarro, F., Langer, N. & Negueruela, I. 2014, *A&A*, 565, A90
 Clark, J. S., Lohr, M. E., Najarro, F., Dong, H. & Martins, F. 2018a, *A&A*, 617, A65
 Clark, J. S., Lohr, M. E., Patrick, L. R. et al. 2018b, *A&A*, 618, A2
 Clark, J. S., Lohr, M. E., Najarro, F., et al. 2018c, *Messenger*, 173, 22
 Clark, J. S., Najarro, F., Negueruela, I. et al. 2019a, *A&A*, 623, A83
 Clark, J. S., Lohr, M. E., Patrick L., & Najarro, F. 2019b, *A&A*, 623, A84
 Clark, J. S., Ritchie, B. W. & Negueruela, I. 2019c, *A&A*, 626, A59
 Clark, J. S., Ritchie, B. W. & Negueruela, I. 2020, 635, A187
 Clark J. S., Patrick L. R., Najarro F., Evans C. J., Lohr M., 2021, *A&A*, 649, A43
 Clarkson, W. I., Ghez, A. M., Morris, M. et al. 2012, *ApJ*, 751, 132
 Cotera, A. S., Erickson, E. F., Colgan, S. W. J. et al. 1996, *ApJ*, 461, 750
 Crowther, P. A. & Bohannan, B. 1997, *A&A*, 317, 532
 Crowther, P. A., Schnurr, O., Hirschi, R., et al. 2010, *MNRAS*, 408, 731
 Crowther, P. A., Caballeri-Nieves, S. M., Bostroem, K. A. et al. 2016, *MNRAS*, 458, 624
 Davies, B., de la Fuente, D., Najarro, F., et al. 2012a, *MNRAS*, 419, 1860
 Davies, B., Clark, J. S., Trombley, C. et al. 2012b, *MNRAS*, 419, 1871
 Diederik Kruijssen, J. M. & Longmore, S. N. 2013, *MNRAS*, 435, 2598
 De Becker, M. & Ruacq, F., 2013, *A&A*, 558, A28
 de Koter A., Heap S. R., Hubeny I., 1997, *ApJ*, 477, 792
 de Koter A., Heap S. R., Hubeny I., 1998, *ApJ*, 509, 879
 de la Fuente, D., Najarro, F., Davies, B., & Figer, D. F. 2013, *Highlights of Spanish Astrophysics VII, Proceedings of the X Scientific Meeting of the Spanish Astronomical Society (SEA)*, held in Valencia, July 9 - 13, 2012, Eds.: J.C. Guirado, L.M. Lara, V. Quilis, and J. Gorgas., pp.534-538
 de la Fuente, D., Najarro, F., Borissova, J. et al. 2016, *A&A*, 589, A69

- De Marco, O. & Izzard, R. G. 2017, *PASA*, 34, 1
- de Mink, S. E., Cantiello, M., Langer, N. et al. 2009, *A&A*, 497, 243
- de Mink, S. E., Sana, H., Langer, N., Izzard, R. G. & Schneider, F. R. N. 2014, *ApJ*, 782, 7
- de Mink, S. E. & Belczynski, K. 2015, *ApJ*, 814, 58
- Deneva, J. S., Cordes, J. M., & Lazio, T. J. W. 2009, *ApJ*, 702, L177
- Doran, E. I., Crowther, P. A., de Koter, A., et al. 2013, *A&A*, 558, A134
- Dougherty, S. M. & Williams, P. M. 2000, *MNRAS*, 319, 1005
- Drissen, L., Lamontagne, R., Moffat, A. F. J., Bastien, P. & Seguin, M. 1986, *ApJ*, 304, 188
- Dunstall, P. R., Dufton, P. L., Sana, H. et al. 2015, *A&A*, 580, A93
- Dworetzky, M. M., 1983, *MNRAS*, 203, 917
- Eisenhauer, F., Abuter, R., Bickert, K., et al. 2003, in *Society of Photo-Optical Instrumentation Engineers (SPIE) Conference Series*, Vol. 4841, Instrument Design and Performance for Optical/Infrared Ground-based Telescopes, ed. M. Iye & A. F. M. Moorwood, 1548-1561
- Eldridge, J. J., Morgan, F., Smartt, S. J., Maund, J. R. & Crockett, R. M. 2013, *MNRAS*, 436, 774
- Eldridge, J. J., Stanway, E. R., Xiao, L. et al. 2017, *PASA*, 34, 58
- Fahed, R. & Moffat, A. F. J. 2012, *MNRAS*, 424, 1601
- Ekström, S., Georgy, C., Eggenberger, P., et al. 2012, *A&A*, 537, A146
- Figer D. F., 1995, *PhDT*
- Figer, D. F., Morris, M., Geballe, T. R. et al. 1999, *ApJ*, 5225, 759
- Figer, D. F., Najarro, F., Gilmore, D. et al. 2002, *ApJ*, 581, 258
- Figer, D. F., 2005, *Nature*, Vol 434, Issue 7030, pp. 192-194.
- Gagne, M., Fehon, G., Savoy, M. R. et al. 2012, *ASPC*, 465, 301
- Gallego-Calvente, A. T., Schödel, R., Alberdi, A. et al. 2021, *A&A*, in press
- Gamen, R., Gosset, E., Morrell, N. I. et al. 2008, *RMxAC*, 33, 119
- Gamen, R., Fernández-Lajús, E., Niemela, V. S., Barbá, R. H. 2009, *A&A*, 506, 1269
- Geballe T. R., Najarro F., Rigaut F., Roy J.-R., 2006, *ApJ*, 652, 370
- Gosset, E., Nazé, Y., Sana, H., Rauw, G., & Vreux, J. -M. 2009, *A&A*, 508, 805
- Gosset, E., & Nazé, Y. 2016, *A&A*, 590, A113
- Gräfener, G. & Hamann, W. -R. 2008, *A&A*, 482, 945
- Gräfener G., 2021, *A&A*, 647, A13
- Groh, J. H., Meynet, G., Ekström, S., & Georgy, C. 2014, *A&A*, 564, A30
- Hamann, F., Depot, D. L. Johansson, S. & Elias, J. 1994, *ApJ*, 422, 626
- Hamann, W.-R., Gräfener, G., & Liermann, A. 2006, *A&A*, 457, 1015
- Hamann, W.-R., Gräfener, Liermann, A., et al. 2019, *A&A*, 625, A57
- Hanson, M. M., Kurt, R., Borissova, J., et al. 2010, *A&A*, 516, A35
- Hillier, D. J. & Miller, D. L. 1998, *ApJ*, 496, 407
- Hillier, D. J. & Miller, D. L. 1999, *ApJ*, 519, 354
- Hillier, D. J., Davidson, K., Ishibashi, K. & Gull, T. 2001, *ApJ*, 553, 837
- Hillier, D. J., Koenigsberger, G., Nazé, Y. et al. 2019, *MNRAS*, 486, 725
- Horne, J. H. & Baliunas, S. L. 1986, *ApJ*, 302, 757
- Huenemoerder, D. P., Schulz, N. S., & Nichols, J. S. 2019, *AJ*, 157, 29
- Humphreys, R. M. & Davidson, K. 1994, *PASP*, 106, 1025
- Hur, H., Sung, H. & Bessell, M. S. 2012, *AJ*, 143, 41
- Ignace, R., Oskinova, L. M., & Follon, C., 2000, *MNRAS*, 318, 214
- Jaque Arancibia, M., Barbá, R. H. & Morrell, M. I. 2015, *BAAA*, 57, 154
- Kobulnicky, H. A., Kiminki, D. C., Lundquist, M. J. et al. 2014, *ApJS*, 213, 34
- Koenigsberger, G., Morrell, N., Hillier, D. J. et al. 2014, *AJ*, 148, 62
- Lamers, H. J. G. L. M. & de Groot, M. J. H. 1992, *A&A*, 257, 153
- Lang, C. C., Goss, W. M. & Rodríguez, L. F. 2001, *ApJ*, 551, L143
- Lang, C. C., Johnson, K. E., Goss, W. M. & Rodríguez, L. F. 2005, *AJ*, 130, 2185
- Lenzen, R., Hartung, M., Brandner, W. et al. 2003, *SPIE*, 4841, 944
- Lépine, S. & Moffat, A. F. J. 1999, 514, 909
- Lohr, M. E., Clark, J. S., Najarro, F., et al. 2018, *A&A*, 617, A66
- Lomb, N. R. 1976, *Ap&SS*, 39, 447
- Luque-Escamilla, P. L., Muñoz-Arjonilla, A. J., Sániche-Sutil, J. R., et al. 2011, *A&A*, 532, A92
- Kennea, J. A., Burrows, D. N., Kouveliotou, C., et al. 2013, *ApJ*, 770, L24
- Mahy, L., Damerdjji, Y., Gosset, E. et al. 2017, *A&A*, 607, A96
- Mahy, L., Sana, H., Abdul-Masih, M. et al. 2020a, *A&A*, 634, A118
- Mahy, L., Almeida, L. A., Sana, H. et al. 2020b, *A&A*, 634, A119
- Maíz Appellániz, Negueruela, I., Barbá, R. H. et al. 2015, *A&A*, 579, A108
- Markakis, K., Bonanos, A. Z., Pietrzynski, G., Macri, L. & Stanek, K. Z., 2011, in Neiner C., Wade G., Meynet G., Peters G., eds, *Proc. IAU Symp. Vol. 272, Active OB stars: structure, evolution, mass loss and critical limits*. p. 298
- Markakis, K., Bonanos, A. Z., Pietrzynski, G., Macri, L., Stanek, K. Z., 2012, in Richards M. T., Hubeny I., eds, *Proc. IAU Symp. Vol. 282, From interacting binaries to exoplanets: essential modeling tools*. p. 454
- Martins, F., Hillier, D. J., Paumard, T. et al. 2008, *A&A*, 478, 219
- Mason, B. D., Hatkopf, W. I., Gies, D. R., Henry, T. J. & Helsel, J. W. 2009, *AJ*, 137, 3358
- Mehner, A., Davidson, K., Ferland, G. J. & Humphreys, R. M. 2010, *ApJ*, 710, 729
- Messineo, M., Davies, B., Ivanov, V. D., et al. 2009, *ApJ*, 697, 701
- Messineo, M., Davies, B., Figer, D. F. et al. 2011, *ApJ*, 733, 41
- Mikles, V. J., Eikenberry, S. S., Muno, M. P., Bandyopadhyay, R. M. & Patel, S. 2006, *ApJ*, 651, 408
- Mikles, V. J., Eikenberry, S. S., Bandyopadhyay, R. M. & Muno, M. P. 2008, *ApJ*, 689, 1222
- Moe, M. & Di Stefano, R. 2017, *ApJS*, 230, 15
- Moffat, A. F. J., Corcoran, M. F., Stevens, I. R., et al. 2002, *ApJ*, 573, 191
- Moffat, A. F. J., Poitras, V., Marchenko, S. V. et al. 2004, *AJ*, 128, 2854
- Moneti, A., Stolovy, Blommaert, J. A. D. L. et al. 2001, *A&A*, 366, 106
- Montes, G., Pérez-Torres, M. A., Alberdi, A., & González, R. F. 2009, *ApJ*, 705, 899
- Montes, G., Ramirez-Ruiz, E., De Colle, F. & Strickler, R. 2013, *ApJ*, 777, 2
- Munoz, M., Moffat, A. F. J., Hill, G. M., et al. 2017, *MNRAS*, 467, 3105
- Nagata, T., Woodward, C. E., Shure, M. & Kobayashi, N. 1995, *AJ*, 109, 1676
- Najarro, F., Figer, D. F., Hillier, D. J. & Kudritzki, R. P., 2004, *ApJL*, 611, 105
- Najarro, F., Figer, D. F., Hillier, D. J. et al. 2009, *ApJ*, 691, 1816
- Nazé, Y., Rauw, G. & Manfroid, 2008, *A&A*, 483, 171
- Nazé, Y., Rauw, G., Sana, H. & Corcoran, M. F. 2013, *A&A*, 555, A83
- Nazé, Y., Gosset, E. & Marechal, Q. 2020, *MNRAS*, tmp, 3587
- Negueruela, I., Clark, J. S., & Ritchie, B. W. 2010, *A&A*, 514, A87
- Niemela, V. S. 1982, *IAUS*, 99 299
- Niemela, V. S. & Gamen, R. C. 2000, *A&A*, 362, 973
- Niemela, V., Seggewiss, W., & Moffat, A. F. J. 2001, *A&A*, 369, 544
- Niemela, V. S., Gamen, R. C., Barbá, R. H., et al. 2008, *MNRAS*, 389, 1447
- Nogueras-Lara, F., Gallego-Calvente, A. T., Dong, H. et al. 2018, *A&A*, 610, 83
- Nogueras-Lara F., Schödel R., Neumayer N., et al. 2020, *A&A*, 641, A141
- Oskinova, L. M. 2005, *MNRAS*, 361, 679
- Oskinova L. M., 2015, in Hamann W., Sander A., Todt H., eds, *Wolf-Rayet Stars: Proceedings of an International Workshop held in Potsdam, Germany, 1.-5. June 2015*. p. 295
- Oskinova L. M., 2016, *Advances in Space Research*, 58, 739
- Parkin, E. R. & Gosset, E. 2011, *A&A*, 530, A119
- Patrick L. R., Lennon D. J., Evans C. J., et al., 2020, *A&A*, 635, A29
- Patrick L. R., Lennon D. J., Britavskiy N., et al., 2019, *A&A*, 624, A129
- Pittard, J. M. & Dawson, B. 2018, *MNRAS*, 477, 5640
- Podsiadlowski, P., Ivanova, N., Justham, S. & Rappaport, S. 2010, *MNRAS*, 406, 840
- Polcaro, V. F., Maryeva, O., Nesci, R. Et al. 2016, *AJ*, 151, 149
- Pollock A. M. T., Haberl F., Corcoran M. F., 1995, in van der Hucht K. A., Williams P. M., eds, *Proc. IAU Symp. 163, Wolf-Rayet Stars: Binaries, Colliding Winds, Evolution*. Kluwer, Dordrecht, p. 191
- Pollock, A. M. T. & Corcoran, M. F. 2006, *A&A*, 445, 1093
- Pollock, A. M. T., Crowther, P. A., Tehrani, K., Broos, P. S. & Townsley, L. K. 2018, *MNRAS*, 474, 3228
- Ponti, G., Morris, M. R., Terrier, R. et al. 2015, *MNRAS*, 453, 172
- Portegies Zwart, S. F., Pooley, D., & Lewin, W. H. G. 2002, *ApJ*, 574, 762
- Portegies Zwart, S. F. & van den Heuvel, E. P. J. 2016, *MNRAS*, 456, 3401
- Pfuhl, O., Alexander, T., Gillessen, S. et al. 2014, *ApJ*, 782, 101
- Raassen, A. J. J. van der Hucht, K. A., Mewe, R. et al. 2003, *A&A*, 402, 653
- Rahoui, F., Tomsick, J. A., Fornasini, F. M., Bodaghee, A., & Bauer, F. E. 2014, *A&A*, 568, A54
- Rate, G. & Crowther, P. A. 2020a, *MNRAS*, 493, 1512
- Rate, G., Crowther, P. A., & Parker, R. J. 2020b, *MNRAS*, 495, 1209

Rauw, G., Vreux, J. -M., Gosset, E. et al. 1996, *A&A*, 306, 771
 Rauw, G., De Becker, M., Nazé, Y. et al. 2004, *A&A*, 420, L9
 Rauw, G., Crowther, P. A., De Becker, M. et al. 2005, *A&A*, 432, 985
 Rauw, G., Sana, H., Nazé, Y. 2011, *A&A*, 535, A40
 Rauw, G., Nazé, Y., Wright, N. J. et al. 2015, *ApJS*, 221, 1
 Ritchie, B. W., Clark J. S., Negueruela, I. & Crowther, P. A. 2009, *A&A*, 507, 1585
 Ritchie, B. W., Clark J. S., Negueruela, I. & Najarro, F. 2021, *A&A* (in press)
 Roman-Lopes, A., Barba, R. H. & Morrel, N. I. 2011, *MNRAS*, 416, 501
 Roman-Lopes, A. 2012, *MNRAS*, 427, L65
 Roman-Lopes, A. 2013, *MNRAS*, 433, 712
 Rousset, G., Lacombe, F., Puget, P. et al. 2003, in Wizinowich P. L., Bonaccini D., eds, *SPIE Conf. Ser. Vol. 4839, Adaptive Optical System Technologies II*. p. 140
 Sana, H., de Mink, S. E., de Koter, A. et al. 2012, *Science*, 337, 444
 Sana, H., de Koter, A., de Mink, S. E., et al. 2013a, *A&A*, 550, A107
 Sana, H., van Boeckel, T., Tramper, F. et al. 2013b, *MNRAS*, 432, L26
 Sana, H., Le Bouquin, J.-B., Lacour, S. et al. 2014, *ApJS*, 215, 15
 Sana, H. 2017, *IAUS*, 329, 110
 Scargle, J. D., 1982, *ApJ*, 263, 835
 Schneider, F. R. N., Izzard, R. G., de Mink, S. E., et al. 2014, *ApJ*, 780, 117
 Schnurr, O., Casoli, J. Chené, A.-N., Moffat, A. F. J. & St-Louis, N., 2008a, *MNRAS*, 389, L38
 Schnurr, O., Moffat, A. F. J., St-Louis, N., Morrell, N. I. & Guerrero, M. A. 2008b, *MNRAS*, 389, 806
 Schnurr, O., Moffat, A. F. J., Villar-Sbaffi, A., St-Louis, N. & Morrell, N. I. 2009a, *MNRAS*, 395, 823
 Schnurr, O., Chené, A. -N., Casoli, J. Moffat, A. F. J. & St-Louis, N. 2009b, *MNRAS*, 397, 2049
 Schweickhardt, J. Schmutz, W., Stahl, O., Szeifert, Th. & Wolf, B. 1999, *A&A*, 347, 127
 Sharples, R., Bendner, R., Agudo Berbel, A., et al. 2013, *Messenger*, 151, 21
 Shenar, T., Richardson, N. D., Sablowski, D. P., et al. 2017, *A&A*, 598, A85
 Shenar, T., Sana, H., Marchant, P. et al. 2021, *A&A*, 650, A147
 Sota, A., Maíz Apellániz, J., Morrell, N. I. et al. 2014, *ApJS*, 211, 10
 Skinner, S. L., Zhekov, S. A., Güdel, M., Schmutz, W. & Kimberly, R. 2010, *AJ*, 139, 825
 Skinner, S. L., Svetozar, A. Z., Güdel, M., Schmutz, W. & Sokal, K. R. 2012, *AJ*, 143, 116
 Smith, N., Gehrz, R., Hinz, P. M. et al. 2003, *AJ*, 125, 1458
 Smith, N. 2006, *MNRAS*, 367, 763
 Smith, N. & Frew, D. J. 2011, *MNRAS*, 415, 2009
 Stevens, I. R., Blondin, J. M. & Pollock, A. M. T. 1992, *ApJ*, 386, 265
 Stevens, I. R. & Howarth, I. D. 1999, *MNRAS*, 302, 549
 Stevenson, S., Sampson, M., Powell, J., et al. 2019, *ApJ*, 882, 121
 St-Louis, N., Chené, A.-N., Schnurr, O. & Nicol, M.-H. 2009, *ApJ*, 698, 1951
 Stroud, V. E., Clark, J. S., Negueruela, I. et al. 2010, *A&A*, 511, A84
 Taylor, W. D., Evans, C. J., Sana, H. et al. 2011, *A&A*, 530, L10
 Tehrani, K. A., Crowther, P. A., Bestenlehner, J. M. et al. 2019, *MNRAS*, 484, 2692
 Tramper, F., Sana, H., Fitzsimons, N. E. et al. 2016, *MNRAS*, 455, 1275
 Townsley, L. K., Broos, P. S., Feigelson, E. D., Garmire, G. P., & Getman, K. V. 2006, *AJ*, 131, 2164
 Townsley, L. K., Broos, P. S., Garmire G. P. & Povich, M. S. 2019, *ApJS*, 244, 28
 Van Loo, S., Runacres, M. C. & Blomme, R. 2006, *A&A*, 452, 1011
 Vigna-Gómez, A., Justham, S., Mandel, I., de Mink, S. E. & Podsiadlowski, P. 2019, *ApJ*, 876, L29
 Wang Q. D., Dong H., & Lang C., 2006, *MNRAS*, 371, 38
 Williams, P. M., van der Hucht, Pollock, A. M. T. et al. 1990, *MNRAS*, 243, 662
 Woosley, S. E., Sukhbold, T. & Janka, H.-T. 2020, *ApJ*, 896, 56
 Wright, A. E. & Barlow, M. J. 1975, *MNRAS*, 170, 41
 Zhekov, S. A. 2012, *MNRAS*, 422, 1332
 Zhekov, S. A. 2017, *MmSAI*, 88, 852

APPENDIX A: OBSERVING LOG AND PRESENTATION OF RV MEASUREMENTS

Table A1 contains the observing log and RV measurements for all epochs for all targets.

APPENDIX B: THE LBV PHENOMENON AND SECULAR VARIABILITY WITHIN THE ARCHES

As massive stars transition away from the Main Sequence they appear to encounter an instability of unknown origin: the so-called luminous blue variable (LBV) phase. Historically it has been thought that the extreme mass loss that characterises LBVs helps facilitate the formation of H-depleted WRs, although observations of Romano's star (Clark et al. (2012), Polcaro et al. (2016)) and the erupting component of the eclipsing hierarchical system HD5980 indicate this behaviour may also be present in WN-subtype WRs. The LBV phenomenon appears to extend to very high masses, with the LBV component of HD5980 having a dynamical mass of $M_{\text{current}} \sim 60M_{\odot}$, implying $M_{\text{initial}} > 80M_{\odot}$ (Koenigsberger et al. (2014); Hillier et al. (2019)). However, this extreme is exceeded by that of the primary in the binary η Carinae, which is generally supposed to be $> 100M_{\odot}$ (Hillier et al. (2001)), with a mass of $\sim 40 - 60M_{\odot}$ suggested for the unseen secondary (Mehner et al. (2010)). η Carinae has been the subject of intensive observation due to both its current exceptional properties and its unprecedented eruption in the 19th Century, during which a luminosity of $\geq 10^7 L_{\odot}$ and a mass loss rate of $\geq 0.5M_{\odot} \text{ yr}^{-1}$ have been inferred (Smith et al. (2003)).

η Carinae is located within the Trumpler 16 + Collinder 228 cluster aggregate, for which Smith ((2006)) infers an age of 2-3Myr. As such - although of significantly lower integrated mass - it appears directly comparable to the Arches; indeed it hosts three WNLha stars, a single O4 supergiant and a number of mid-O giants and main sequence stars (cf. papers I and III). Given this similarity one might ask whether the Arches hosts any star exhibiting the LBV phenomenon? Trivially, despite the presence of similarly massive binaries within the Arches, there appears to be no direct analogue of η Carinae; its K-band morphology is very different from any cluster member (Hamann et al. (1994)), while any nebula comparable to the Homunculus would be clearly visible (cf. the Pistol nebula; Figer et al. (1999)).

Surprisingly, none of the stars within our sample showed any evidence of long term changes in their spectral morphologies during this period. Simulations of $60M_{\odot}$ stars by Groh et al. ((2014)) predict that the LBV phenomenon occurs directly after a late-O/early-B hypergiant phase around $\geq 3\text{Myr}$, implying that the cohort of mid-O supergiants and, potentially, the mid- to late-hypergiants have yet to reach this evolutionary juncture. Unfortunately no predictions exist for when, or even if, more massive stars such as the Arches WNLha cohort become LBVs, nor how long this episode endures. Given the limited cadence of the observations, one could imagine that if the outbursts/eruption duty cycle were long, or outbursts rapid, they could have been missed. Indeed, while η Carinae was highly (photometrically) active throughout the 19th and 20th Centuries (Smith & Frew (2011)) and the characteristic variability of LBVs occurs over months to years (e.g. Humphreys & Davidson (1994)), observations of P Cygni reveal that LBVs may reside in a quiescent state for centuries (cf. Lamers & de Groot (1992)). Alternatively one might suppose that WNLha stars have yet to reach the LBV phase, or that such stars circumvent it entirely. However such a hypothesis would require the 19th Century eruption of η Carina to be driven by a mechanism other than the nuclear evolution of the star, such as binary interaction/merger (Portegies Zwart & van den Heuvel (2015)).

Table A1. Dates of epochs of observation for Arches sample and associated RV measurements

Star	Instrument	Epochs of observations (and associated RV measurements)
B1	Sinfoni	10/06/05 ($0.21 \pm 3.05 \text{ km s}^{-1}$), 08/08/13 ($-2.95 \pm 2.97 \text{ km s}^{-1}$), 21/04/17 ($0.09 \pm 2.35 \text{ km s}^{-1}$), 26/04/17 ($0.07 \pm 3.16 \text{ km s}^{-1}$), 30/04/17 ($2.58 \pm 3.30 \text{ km s}^{-1}$)
	KMOS	30/04/14 ($-3.60 \pm 5.96 \text{ km s}^{-1}$), 23/07/14 ($2.86 \pm 9.78 \text{ km s}^{-1}$), 04/08/14 ($11.31 \pm 15.10 \text{ km s}^{-1}$), 05/08/14 ($-7.02 \pm 6.55 \text{ km s}^{-1}$), 11/08/14 ($1.03 \pm 5.97 \text{ km s}^{-1}$), 12/08/14 ($-10.32 \pm 5.89 \text{ km s}^{-1}$), 13/08/14 ($5.75 \pm 7.25 \text{ km s}^{-1}$)
F1	Sinfoni	10/06/05 ($-6.43 \pm 6.53 \text{ km s}^{-1}$), 29/06/11 ($4.70 \pm 5.57 \text{ km s}^{-1}$), 27/08/11 ($-9.50 \pm 5.81 \text{ km s}^{-1}$), 28/08/11 ($-1.67 \pm 5.01 \text{ km s}^{-1}$), 17/07/13 ($4.46 \pm 5.38 \text{ km s}^{-1}$), 08/08/13 ($4.70 \pm 5.86 \text{ km s}^{-1}$), 26/04/17 ($2.97 \pm 5.04 \text{ km s}^{-1}$), 30/04/17 ($-5.45 \pm 5.55 \text{ km s}^{-1}$), 26/07/17 ($-6.90 \pm 5.49 \text{ km s}^{-1}$), 07/05/18 ($-9.93 \pm 7.01 \text{ km s}^{-1}$), 07/08/18 ($4.85 \pm 6.66 \text{ km s}^{-1}$), 10/08/18 ($4.73 \pm 9.26 \text{ km s}^{-1}$), 12/08/18 ($11.38 \pm 7.61 \text{ km s}^{-1}$), 17/08/18 ($2.07 \pm 4.94 \text{ km s}^{-1}$)
	KMOS	12/08/14 ($-2.95 \pm 3.13 \text{ km s}^{-1}$), 13/08/14 ($2.95 \pm 3.13 \text{ km s}^{-1}$)
F2	Sinfoni	10/06/05 ($-16.05 \pm 8.22 \text{ km s}^{-1}$), 29/06/11 ($-230.15 \pm 8.26 \text{ km s}^{-1}$), 27/08/11 ($96.20 \pm 7.19 \text{ km s}^{-1}$), 28/08/11 ($-85.25 \pm 11.19 \text{ km s}^{-1}$), 17/07/13 ($130.44 \pm 6.78 \text{ km s}^{-1}$), 08/08/13 ($104.81 \pm 7.10 \text{ km s}^{-1}$)
	KMOS	30/04/14 ($-70.04 \pm 14.07 \text{ km s}^{-1}$), 23/07/14 ($-44.94 \pm 12.45 \text{ km s}^{-1}$), 04/08/14 ($-56.15 \pm 11.73 \text{ km s}^{-1}$), 05/08/14 ($-0.05 \pm 12.62 \text{ km s}^{-1}$), 11/08/14 ($198.74 \pm 11.38 \text{ km s}^{-1}$), 12/08/14 ($54.41 \pm 16.62 \text{ km s}^{-1}$), 13/08/14 ($-81.97 \pm 11.56 \text{ km s}^{-1}$)
F3	Sinfoni	10/06/05 ($-4.81 \pm 4.39 \text{ km s}^{-1}$), 08/08/13 ($1.29 \pm 2.39 \text{ km s}^{-1}$), 21/04/17 ($4.98 \pm 2.33 \text{ km s}^{-1}$), 26/04/17 ($-1.88 \pm 2.78 \text{ km s}^{-1}$), 30/04/17 ($-0.60 \pm 2.31 \text{ km s}^{-1}$), 08/08/18 ($2.42 \pm 3.11 \text{ km s}^{-1}$), 17/08/18 ($-1.39 \pm 2.49 \text{ km s}^{-1}$), 18/08/18 (low S/N)
F4	Sinfoni	29/05/13 ($0.54 \pm 2.19 \text{ km s}^{-1}$), 08/06/13 ($-0.17 \pm 2.16 \text{ km s}^{-1}$), 17/07/13 ($-6.78 \pm 2.50 \text{ km s}^{-1}$), 03/08/13 ($-3.57 \pm 1.79 \text{ km s}^{-1}$), 04/08/13 ($-2.21 \pm 1.99 \text{ km s}^{-1}$), 06/08/13 ($-4.98 \pm 2.66 \text{ km s}^{-1}$), 08/08/13 ($12.66 \pm 2.63 \text{ km s}^{-1}$), 26/04/17 ($4.75 \pm 2.18 \text{ km s}^{-1}$), 30/04/17 ($0.10 \pm 1.76 \text{ km s}^{-1}$), 27/07/17 ($-0.33 \pm 1.95 \text{ km s}^{-1}$)
F5	Sinfoni	10/06/05 ($0.93 \pm 3.14 \text{ km s}^{-1}$), 08/08/13 ($-7.49 \pm 1.92 \text{ km s}^{-1}$), 21/04/17 ($6.91 \pm 1.77 \text{ km s}^{-1}$), 26/04/17 ($5.32 \pm 2.46 \text{ km s}^{-1}$), 30/04/17 ($4.52 \pm 1.92 \text{ km s}^{-1}$), 08/08/18 ($-1.70 \pm 1.98 \text{ km s}^{-1}$), 18/08/18 ($-8.51 \pm 2.09 \text{ km s}^{-1}$)
F6	Sinfoni	14/04/11 ($-17.17 \pm 6.31 \text{ km s}^{-1}$), 17/07/13 ($-4.28 \pm 4.19 \text{ km s}^{-1}$), 26/04/17 ($-9.37 \pm 3.92 \text{ km s}^{-1}$), 30/04/17 ($15.87 \pm 3.99 \text{ km s}^{-1}$), 26/07/17 ($-8.94 \pm 5.00 \text{ km s}^{-1}$), 07/05/18 ($-14.99 \pm 5.11 \text{ km s}^{-1}$), 07/08/18 ($-11.45 \pm 4.95 \text{ km s}^{-1}$), 12/08/18 ($50.44 \pm 6.40 \text{ km s}^{-1}$), 17/08/18 ($-1.19 \pm 3.96 \text{ km s}^{-1}$), 18/08/18 ($1.08 \pm 3.99 \text{ km s}^{-1}$)
	KMOS	30/04/14 ($-0.44 \pm 11.38 \text{ km s}^{-1}$), 23/07/14 ($7.78 \pm 12.98 \text{ km s}^{-1}$), 04/08/14 ($26.05 \pm 12.73 \text{ km s}^{-1}$), 05/08/14 ($27.41 \pm 15.40 \text{ km s}^{-1}$), 11/08/14 ($-28.18 \pm 12.95 \text{ km s}^{-1}$), 12/08/14 ($-16.96 \pm 10.10 \text{ km s}^{-1}$), 13/08/14 ($-15.66 \pm 14.04 \text{ km s}^{-1}$)
F7	Sinfoni	29/05/13 ($17.56 \pm 2.93 \text{ km s}^{-1}$), 18/06/13 ($17.01 \pm 3.86 \text{ km s}^{-1}$), 17/07/13 ($5.76 \pm 3.09 \text{ km s}^{-1}$), 03/08/13 ($5.61 \pm 3.39 \text{ km s}^{-1}$), 04/08/13 ($22.99 \pm 3.03 \text{ km s}^{-1}$), 06/08/13 ($9.57 \pm 3.05 \text{ km s}^{-1}$), 08/08/13 ($19.13 \pm 3.24 \text{ km s}^{-1}$), 26/04/17 ($-17.26 \pm 2.98 \text{ km s}^{-1}$), 30/04/17 ($-12.43 \pm 2.89 \text{ km s}^{-1}$), 27/07/17 ($-20.84 \pm 3.10 \text{ km s}^{-1}$), 07/05/18 ($-6.31 \pm 4.31 \text{ km s}^{-1}$), 07/08/18 ($-12.14 \pm 2.77 \text{ km s}^{-1}$), 12/08/18 ($-8.22 \pm 2.62 \text{ km s}^{-1}$), 17/08/18 ($-12.72 \pm 3.49 \text{ km s}^{-1}$), 18/08/18 ($-7.70 \pm 3.00 \text{ km s}^{-1}$)
F8	Sinfoni	14/04/11 ($-12.36 \pm 3.78 \text{ km s}^{-1}$), 17/07/13 ($5.21 \pm 2.73 \text{ km s}^{-1}$), 06/08/13 ($8.15 \pm 2.67 \text{ km s}^{-1}$), 26/04/17 ($9.34 \pm 3.41 \text{ km s}^{-1}$), 30/04/17 ($12.12 \pm 2.33 \text{ km s}^{-1}$), 07/05/18 ($-1.91 \pm 2.85 \text{ km s}^{-1}$), 07/08/18 ($-0.95 \pm 2.30 \text{ km s}^{-1}$), 12/08/18 ($-8.83 \pm 2.56 \text{ km s}^{-1}$), 17/08/18 ($-3.95 \pm 2.66 \text{ km s}^{-1}$), 18/08/18 ($-6.81 \pm 2.35 \text{ km s}^{-1}$)
	KMOS	30/04/14 ($-3.60 \pm 5.96 \text{ km s}^{-1}$), 23/07/14 ($2.86 \pm 9.78 \text{ km s}^{-1}$), 04/08/14 ($11.31 \pm 15.10 \text{ km s}^{-1}$), 05/08/14 ($-7.02 \pm 6.55 \text{ km s}^{-1}$), 11/08/14 ($1.03 \pm 5.97 \text{ km s}^{-1}$), 12/08/14 ($-10.32 \pm 5.89 \text{ km s}^{-1}$), 13/08/14 ($5.75 \pm 7.25 \text{ km s}^{-1}$)
F9	Sinfoni	10/06/05 ($-6.86 \pm 7.18 \text{ km s}^{-1}$), 29/06/11 ($6.97 \pm 4.09 \text{ km s}^{-1}$), 27/08/11 ($-16.60 \pm 5.52 \text{ km s}^{-1}$), 28/08/11 ($3.03 \pm 4.53 \text{ km s}^{-1}$), 17/07/13 ($6.47 \pm 5.00 \text{ km s}^{-1}$), 08/08/13 ($11.26 \pm 5.92 \text{ km s}^{-1}$), 25/04/17 ($-3.35 \pm 4.76 \text{ km s}^{-1}$), 26/04/17 ($2.63 \pm 4.73 \text{ km s}^{-1}$), 30/04/17 ($1.31 \pm 4.66 \text{ km s}^{-1}$), 23/06/17 ($-7.50 \pm 4.62 \text{ km s}^{-1}$), 07/05/18 ($-1.43 \pm 4.54 \text{ km s}^{-1}$), 07/08/18 ($4.97 \pm 4.21 \text{ km s}^{-1}$), 10/08/18 ($0.32 \pm 3.82 \text{ km s}^{-1}$), 12/08/18 ($3.70 \pm 4.30 \text{ km s}^{-1}$), 17/08/18 ($-4.91 \pm 7.48 \text{ km s}^{-1}$)
	KMOS	30/04/14 ($-9.74 \pm 10.15 \text{ km s}^{-1}$), 23/07/14 ($3.85 \pm 9.07 \text{ km s}^{-1}$), 04/08/14 ($0.17 \pm 8.78 \text{ km s}^{-1}$), 05/08/13 ($1.24 \pm 9.85 \text{ km s}^{-1}$), 12/08/14 ($1.38 \pm 7.83 \text{ km s}^{-1}$), 13/08/14 ($3.09 \pm 11.35 \text{ km s}^{-1}$)

Table A1 – *continued* Dates of epochs of observation for Arches sample and associated RV measurements

Star	Instrument	Epochs of observations (and associated RV measurements)
F10	Sinfoni	10/06/05 (-0.31 ± 5.43 km s ⁻¹), 25/04/17 (4.97 ± 3.36 km s ⁻¹), 26/04/17 (0.55 ± 3.41 km s ⁻¹), 30/04/17 (-4.84 ± 3.01 km s ⁻¹), 23/06/17 (-0.61 ± 6.03 km s ⁻¹), 07/05/18 (6.40 ± 4.27 km s ⁻¹), 07/08/18 (2.99 ± 3.32 km s ⁻¹), 10/08/18 (-2.97 ± 3.78 km s ⁻¹), 12/08/18 (-1.93 ± 3.29 km s ⁻¹), 17/08/18 (-4.26 ± 4.88 km s ⁻¹)
F12	Sinfoni	10/06/05 (-8.42 ± 6.20 km s ⁻¹), 29/06/11 (5.47 ± 6.26 km s ⁻¹), 27/08/11 (-0.28 ± 5.79 km s ⁻¹), 28/08/11 (10.62 ± 5.31 km s ⁻¹), 17/07/13 (-0.14 ± 6.85 km s ⁻¹), 03/08/13 (-0.03 ± 6.65 km s ⁻¹), 04/08/13 (low S/N), (06/08/13), 08/08/13 (-1.02 ± 6.04 km s ⁻¹), 26/04/17 (1.72 ± 4.41 km s ⁻¹), 30/04/17 (-5.44 ± 4.66 km s ⁻¹), 27/07/17 (-2.48 ± 4.89 km s ⁻¹)
F13	Sinfoni	10/06/05 (-7.19 ± 11.31 km s ⁻¹), 25/04/17 (3.43 ± 6.63 km s ⁻¹), 26/04/17 (16.34 ± 7.68 km s ⁻¹), 30/04/17 (-0.93 ± 7.78 km s ⁻¹), 23/06/17 (0.10 ± 6.97 km s ⁻¹), 07/05/18 (-13.19 ± 6.80 km s ⁻¹), 07/08/18 (-2.96 ± 6.84 km s ⁻¹), 10/08/18 (-4.21 ± 6.72 km s ⁻¹), 12/08/18 (8.61 ± 6.24 km s ⁻¹)
F14	Sinfoni	14/04/11 (-11.98 ± 3.20 km s ⁻¹), 17/07/13 (-8.51 ± 2.68 km s ⁻¹), 26/04/17 (15.39 ± 2.75 km s ⁻¹), 30/04/17 (20.40 ± 2.96 km s ⁻¹), 26/07/17 (-6.61 ± 3.51 km s ⁻¹), 07/05/18 (6.49 ± 3.97 km s ⁻¹), 07/08/18 (3.44 ± 3.25 km s ⁻¹), 08/08/18 (0.60 ± 3.03 km s ⁻¹), 12/08/18 (-3.77 ± 2.68 km s ⁻¹), 17/08/18 (-12.41 ± 2.55 km s ⁻¹), 18/08/18 (-3.04 ± 2.85 km s ⁻¹)
F15	Sinfoni	29/05/13 (28.79 ± 4.21 km s ⁻¹), 18/06/13 (-1.63 ± 6.15 km s ⁻¹), 17/07/13 (-39.28 ± 4.47 km s ⁻¹), 03/08/13 (13.99 ± 4.17 km s ⁻¹), 04/08/13 (16.52 ± 3.74 km s ⁻¹), 06/08/13 (15.26 ± 4.20 km s ⁻¹), 08/08/13 (13.31 ± 5.41 km s ⁻¹), 26/04/17 (35.95 ± 4.93 km s ⁻¹), 30/04/17 (25.80 ± 3.41 km s ⁻¹), 23/06/17 (-8.32 ± 3.80 km s ⁻¹), 27/07/17 (24.97 ± 3.78 km s ⁻¹), 07/05/18 (-42.62 ± 3.66 km s ⁻¹), 07/08/18 (-38.63 ± 4.07 km s ⁻¹), 12/08/18 (-26.95 ± 3.80 km s ⁻¹), 17/08/18 (-5.37 ± 5.57 km s ⁻¹), 18/08/18 (-11.78 ± 3.68 km s ⁻¹)
F16	Sinfoni	14/04/11 (0.01 ± 3.81 km s ⁻¹), 17/07/13 (-0.06 ± 3.83 km s ⁻¹), 06/08/13 (-5.03 ± 3.45 km s ⁻¹), 26/04/17 (-10.82 ± 2.92 km s ⁻¹), 30/04/17 (1.68 ± 3.57 km s ⁻¹), 07/05/18 (2.66 ± 3.73 km s ⁻¹), 07/08/18 (-1.00 ± 2.97 km s ⁻¹), 12/08/18 (15.14 ± 3.30 km s ⁻¹), 17/08/18 (-5.03 ± 2.98 km s ⁻¹), 18/08/18 (2.45 ± 3.24 km s ⁻¹)
	KMOS	30/04/14
F17	Sinfoni	10/06/05 (2.23 ± 6.08 km s ⁻¹), 25/04/17 (-1.93 ± 5.02 km s ⁻¹), 26/04/17 (2.40 ± 4.31 km s ⁻¹), 30/04/17 (10.94 ± 6.02 km s ⁻¹), 23/06/17 (-9.53 ± 4.55 km s ⁻¹), 07/05/18 (-8.14 ± 6.21 km s ⁻¹), 07/08/18 (1.92 ± 4.01 km s ⁻¹), 10/08/18 (-9.03 ± 4.27 km s ⁻¹), 12/08/18 (1.93 ± 4.58 km s ⁻¹), 17/08/18 (9.21 ± 5.19 km s ⁻¹)
B4	Sinfoni	29/05/13 (-0.65 ± 9.68 km s ⁻¹), 18/06/13 (-5.08 ± 5.43 km s ⁻¹), 17/07/13 (-7.77 ± 6.16 km s ⁻¹), 03/08/13 (13.27 ± 4.95 km s ⁻¹), 04/08/13 (5.50 ± 4.82 km s ⁻¹), 06/08/13 (-10.01 ± 5.40 km s ⁻¹), 08/08/13 (-6.80 ± 6.59 km s ⁻¹), 26/04/17 (7.74 ± 6.32 km s ⁻¹), 30/04/17 (2.76 ± 4.82 km s ⁻¹), 27/07/17 (2.48 ± 6.25 km s ⁻¹), 17/08/18 (-1.44 ± 5.56 km s ⁻¹)
F18	Sinfoni	29/05/13 (14.15 ± 7.14 km s ⁻¹), 18/06/13 (13.40 ± 7.66 km s ⁻¹), 17/07/13 (1.61 ± 5.14 km s ⁻¹), 03/08/13 (-0.02 ± 5.67 km s ⁻¹), 04/08/13 (-9.13 ± 5.09 km s ⁻¹), 06/08/13 (-7.85 ± 5.05 km s ⁻¹), 08/08/13 (-18.23 ± 4.96 km s ⁻¹), 26/04/17 (13.94 ± 5.01 km s ⁻¹), 30/04/17 (8.56 ± 5.11 km s ⁻¹), 27/07/17 (-16.42 ± 5.72 km s ⁻¹)
F19	Sinfoni	10/06/05 (low S/N), 29/06/11 (low S/N), 27/08/11 (low S/N), 17/07/13 (low S/N), 08/08/13 (low S/N)
F20	Sinfoni	29/05/13 (0.77 ± 8.91 km s ⁻¹), 18/06/13 (0.62 ± 14.07 km s ⁻¹), 17/07/13 (7.06 ± 8.18 km s ⁻¹), 03/08/13 (-10.50 ± 7.35 km s ⁻¹), 04/08/13 (-14.15 ± 8.00 km s ⁻¹), 06/08/13 (-15.23 ± 7.31 km s ⁻¹), 08/08/13 (-1.34 ± 8.69 km s ⁻¹), 26/04/17 (15.40 ± 7.17 km s ⁻¹), 30/04/17 (-4.29 ± 6.67 km s ⁻¹), 27/07/17 (low S/N), 07/05/18 (-0.13 ± 7.67 km s ⁻¹), 07/08/18 (1.10 ± 8.29 km s ⁻¹), 12/08/18 (5.18 ± 9.45 km s ⁻¹), 17/08/18 (4.79 ± 9.39 km s ⁻¹), 18/08/18 (10.73 ± 6.66 km s ⁻¹)

Table A1 – continued Dates of epochs of observation for Arches sample and associated RV measurements

Star	Instrument	Epochs of observations (and associated RV measurements)
F21	Sinfoni	29/05/13 ($5.77 \pm 6.65 \text{ km s}^{-1}$), 18/06/13 ($7.08 \pm 10.76 \text{ km s}^{-1}$), 17/07/13 ($-10.74 \pm 6.74 \text{ km s}^{-1}$), 03/08/13 ($-6.53 \pm 9.81 \text{ km s}^{-1}$), 04/08/13 ($-7.02 \pm 5.52 \text{ km s}^{-1}$), 06/08/13 ($-12.92 \pm 6.37 \text{ km s}^{-1}$), 08/08/13 ($-9.74 \pm 7.97 \text{ km s}^{-1}$), 26/04/17 ($7.19 \pm 5.54 \text{ km s}^{-1}$), 30/04/17 ($-0.20 \pm 6.25 \text{ km s}^{-1}$), 27/07/17 ($4.62 \pm 7.15 \text{ km s}^{-1}$), 07/05/18 ($-11.57 \pm 8.70 \text{ km s}^{-1}$), 07/08/18 ($8.02 \pm 6.95 \text{ km s}^{-1}$), 12/08/18 ($7.55 \pm 7.85 \text{ km s}^{-1}$), 17/08/18 ($-0.34 \pm 6.35 \text{ km s}^{-1}$), 18/08/18 ($18.82 \pm 7.81 \text{ km s}^{-1}$)
F22	Sinfoni	10/06/05 ($-5.10 \pm 5.35 \text{ km s}^{-1}$), 29/06/11 ($-19.16 \pm 5.82 \text{ km s}^{-1}$), 27/08/11 ($8.71 \pm 6.44 \text{ km s}^{-1}$), 28/08/11 ($2.90 \pm 5.41 \text{ km s}^{-1}$), 17/07/13 ($4.54 \pm 6.80 \text{ km s}^{-1}$), 08/08/13 ($-3.38 \pm 5.19 \text{ km s}^{-1}$), 26/04/17 ($4.30 \pm 5.59 \text{ km s}^{-1}$), 30/04/17 ($8.03 \pm 5.85 \text{ km s}^{-1}$), 27/07/17 ($-0.85 \pm 4.93 \text{ km s}^{-1}$)
F23	Sinfoni	10/06/05 ($10.16 \pm 7.14 \text{ km s}^{-1}$), 07/05/18 ($-13.09 \pm 5.62 \text{ km s}^{-1}$), 07/08/18 ($-3.62 \pm 4.92 \text{ km s}^{-1}$), 12/08/18 ($-0.03 \pm 4.79 \text{ km s}^{-1}$), 17/08/18 ($-1.13 \pm 7.85 \text{ km s}^{-1}$), 18/08/18 ($7.71 \pm 5.76 \text{ km s}^{-1}$)
F24	Sinfoni	10/06/05 (low S/N), 29/06/11 (low S/N), 27/08/11 ($-12.15 \pm 10.03 \text{ km s}^{-1}$), 28/08/11 (low S/N), 17/07/13 (low S/N), 08/08/13 (low S/N), 07/08/18 ($13.23 \pm 8.42 \text{ km s}^{-1}$), 10/08/18 ($8.28 \pm 7.69 \text{ km s}^{-1}$), 12/08/18 ($3.17 \pm 6.79 \text{ km s}^{-1}$), 17/08/18 ($-12.54 \pm 5.73 \text{ km s}^{-1}$)
F25	Sinfoni	10/06/05 ($95.71 \pm 13.49 \text{ km s}^{-1}$), 29/06/11 ($-72.56 \pm 11.84 \text{ km s}^{-1}$), 27/08/11 (low S/N), 17/07/13 ($-20.43 \pm 11.87 \text{ km s}^{-1}$), 08/08/13 ($-43.61 \pm 13.97 \text{ km s}^{-1}$), 25/04/17 ($37.19 \pm 12.57 \text{ km s}^{-1}$), 26/04/17 ($98.02 \pm 8.60 \text{ km s}^{-1}$), 30/04/17 ($-54.12 \pm 9.52 \text{ km s}^{-1}$), 23/06/17 ($-54.47 \pm 10.97 \text{ km s}^{-1}$), 07/05/18 ($-59.07 \pm 9.15 \text{ km s}^{-1}$), 07/08/18 ($-28.04 \pm 10.28 \text{ km s}^{-1}$), 10/08/18 ($54.49 \pm 9.93 \text{ km s}^{-1}$), 12/08/18 ($46.90 \pm 8.21 \text{ km s}^{-1}$)
F26	Sinfoni	10/06/05 ($-12.93 \pm 15.09 \text{ km s}^{-1}$), 14/04/11 ($21.25 \pm 15.09 \text{ km s}^{-1}$), 17/07/13 ($29.97 \pm 14.37 \text{ km s}^{-1}$), 26/04/17 ($5.45 \pm 10.90 \text{ km s}^{-1}$), 26/07/17 ($0.30 \pm 13.88 \text{ km s}^{-1}$), 08/08/18 ($-10.26 \pm 11.38 \text{ km s}^{-1}$), 17/08/18 ($-23.37 \pm 12.76 \text{ km s}^{-1}$), 18/08/18 ($-10.41 \pm 13.26 \text{ km s}^{-1}$)
F27	Sinfoni	29/05/13 ($10.97 \pm 6.74 \text{ km s}^{-1}$), 18/06/13 ($-0.35 \pm 6.96 \text{ km s}^{-1}$), 17/07/13 ($-5.64 \pm 4.99 \text{ km s}^{-1}$), 03/08/13 ($0.73 \pm 6.38 \text{ km s}^{-1}$), 04/08/13 ($7.96 \pm 5.69 \text{ km s}^{-1}$), 06/08/13 ($-6.79 \pm 4.84 \text{ km s}^{-1}$), 08/08/13 ($-10.68 \pm 6.11 \text{ km s}^{-1}$), 26/04/17 ($2.16 \pm 5.13 \text{ km s}^{-1}$), 30/04/17 ($-3.23 \pm 4.77 \text{ km s}^{-1}$), 27/07/17 ($-21.47 \pm 8.01 \text{ km s}^{-1}$), 07/05/18 ($9.45 \pm 5.64 \text{ km s}^{-1}$), 07/08/18 ($5.94 \pm 6.26 \text{ km s}^{-1}$), 12/08/18 ($5.91 \pm 7.38 \text{ km s}^{-1}$), 17/08/18 ($5.03 \pm 6.73 \text{ km s}^{-1}$), 18/08/18 (low S/N)
F28	Sinfoni	14/04/11 ($-21.58 \pm 5.79 \text{ km s}^{-1}$), 17/07/13 ($10.94 \pm 5.29 \text{ km s}^{-1}$), 26/04/17 ($7.48 \pm 5.36 \text{ km s}^{-1}$), 30/04/17 ($2.50 \pm 8.12 \text{ km s}^{-1}$), 26/07/17 ($-0.07 \pm 6.33 \text{ km s}^{-1}$), 07/05/18 ($-13.96 \pm 4.76 \text{ km s}^{-1}$), 07/08/18 ($5.76 \pm 7.18 \text{ km s}^{-1}$), 12/08/18 ($6.00 \pm 5.53 \text{ km s}^{-1}$), 17/08/18 ($-4.67 \pm 5.74 \text{ km s}^{-1}$), 18/08/18 ($7.61 \pm 6.10 \text{ km s}^{-1}$)
F29	Sinfoni	29/05/13 ($-1.21 \pm 6.51 \text{ km s}^{-1}$), 18/06/13 ($3.89 \pm 8.28 \text{ km s}^{-1}$), 17/07/13 ($-7.61 \pm 6.59 \text{ km s}^{-1}$), 03/08/13 ($6.66 \pm 6.11 \text{ km s}^{-1}$), 04/08/13 ($-1.40 \pm 6.04 \text{ km s}^{-1}$), 06/08/13 ($-20.30 \pm 5.88 \text{ km s}^{-1}$), 08/08/13 ($-3.31 \pm 7.56 \text{ km s}^{-1}$), 26/04/17 ($-1.28 \pm 5.29 \text{ km s}^{-1}$), 30/04/17 ($1.04 \pm 4.63 \text{ km s}^{-1}$), 23/06/17 ($8.67 \pm 7.54 \text{ km s}^{-1}$), 27/07/17 ($-10.32 \pm 6.71 \text{ km s}^{-1}$), 07/05/18 ($-3.33 \pm 5.45 \text{ km s}^{-1}$), 07/08/18 ($0.10 \pm 7.26 \text{ km s}^{-1}$), 12/08/18 ($14.70 \pm 5.68 \text{ km s}^{-1}$), 17/08/18 ($-2.47 \pm 8.23 \text{ km s}^{-1}$), 18/08/18 ($16.16 \pm 5.62 \text{ km s}^{-1}$)
F30	Sinfoni	29/06/11 ($-6.89 \pm 7.76 \text{ km s}^{-1}$), 27/08/11 ($0.69 \pm 14.61 \text{ km s}^{-1}$), 28/08/11 ($0.36 \pm 8.24 \text{ km s}^{-1}$), 17/07/13 ($7.20 \pm 7.63 \text{ km s}^{-1}$), 08/08/13 ($-1.68 \pm 7.84 \text{ km s}^{-1}$), 26/04/17 ($4.76 \pm 9.07 \text{ km s}^{-1}$), 30/04/17 ($-3.81 \pm 8.60 \text{ km s}^{-1}$), 27/07/17 ($-0.64 \pm 9.33 \text{ km s}^{-1}$)
F32	Sinfoni	14/04/11 ($-2.03 \pm 5.84 \text{ km s}^{-1}$), 17/07/13 ($-3.07 \pm 5.15 \text{ km s}^{-1}$), 06/08/13 ($-1.79 \pm 6.95 \text{ km s}^{-1}$), 26/04/17 ($9.54 \pm 7.00 \text{ km s}^{-1}$), 30/04/17 ($-2.80 \pm 5.45 \text{ km s}^{-1}$), 07/05/18 ($-9.88 \pm 7.06 \text{ km s}^{-1}$), 07/08/18 ($-17.89 \pm 5.39 \text{ km s}^{-1}$), 12/08/18 ($3.53 \pm 6.78 \text{ km s}^{-1}$), 17/08/18 ($-1.58 \pm 7.42 \text{ km s}^{-1}$), 18/08/18 ($25.97 \pm 6.40 \text{ km s}^{-1}$)
F33	Sinfoni	14/04/11 ($-17.07 \pm 12.70 \text{ km s}^{-1}$), 17/07/13 ($-10.13 \pm 8.76 \text{ km s}^{-1}$), 06/08/13 ($-9.45 \pm 7.39 \text{ km s}^{-1}$), 26/04/17 ($5.78 \pm 7.06 \text{ km s}^{-1}$), 30/04/17 ($13.18 \pm 6.56 \text{ km s}^{-1}$), 07/05/18 ($-15.09 \pm 8.57 \text{ km s}^{-1}$), 07/08/18 ($4.80 \pm 9.40 \text{ km s}^{-1}$), 12/08/18 ($6.61 \pm 7.39 \text{ km s}^{-1}$), 17/08/18 ($0.57 \pm 8.34 \text{ km s}^{-1}$), 18/08/18 ($20.80 \pm 7.59 \text{ km s}^{-1}$)

Table A1 – *continued* Dates of epochs of observation for Arches sample and associated RV measurements

Star	Instrument	Epochs of observations (and associated RV measurements)
F34	Sinfoni	14/04/11 (-11.79 ± 6.68 km s ⁻¹), 17/07/13 (2.46 ± 5.90 km s ⁻¹), 06/08/13 (-17.65 ± 5.79 km s ⁻¹), 26/04/17 (3.30 ± 4.74 km s ⁻¹), 30/04/17 (3.44 ± 6.79 km s ⁻¹), 07/05/18 (-2.51 ± 6.28 km s ⁻¹), 07/08/18 (5.68 ± 8.82 km s ⁻¹), 12/08/18 (1.54 ± 6.28 km s ⁻¹), 17/08/18 (1.40 ± 5.21 km s ⁻¹), 18/08/18 (14.12 ± 7.93 km s ⁻¹)
F35	Sinfoni	29/05/13 (-9.87 ± 13.87 km s ⁻¹), 18/06/13 (-85.16 ± 14.84 km s ⁻¹), 17/07/13 (-76.45 ± 14.20 km s ⁻¹), 03/08/13 (142.45 ± 13.46 km s ⁻¹), 04/08/13 (-55.16 ± 11.97 km s ⁻¹), 06/08/13 (-60.85 ± 11.18 km s ⁻¹), 08/08/13 (55.56 ± 14.31 km s ⁻¹), 26/04/17 (-60.49 ± 12.60 km s ⁻¹), 30/04/17 (8.06 ± 12.00 km s ⁻¹), 23/06/17 (134.17 ± 12.05 km s ⁻¹), 27/07/17 (-41.69 ± 19.00 km s ⁻¹), 07/05/18 (4.08 ± 10.95 km s ⁻¹), 07/08/18 (97.23 ± 13.10 km s ⁻¹), 12/08/18 (14.03 ± 11.51 km s ⁻¹), 17/08/18 (-73.13 ± 10.93 km s ⁻¹), 18/08/18 (7.22 ± 14.25 km s ⁻¹)
F38	Sinfoni	14/04/11 (-3.69 ± 5.60 km s ⁻¹), 17/07/13 (-14.65 ± 6.12 km s ⁻¹), 06/08/13 (-14.28 ± 5.89 km s ⁻¹), 26/04/17 (2.17 ± 5.99 km s ⁻¹), 30/04/17 (-7.13 ± 5.11 km s ⁻¹), 07/05/18 (5.92 ± 5.13 km s ⁻¹), 07/08/18 (6.23 ± 5.40 km s ⁻¹), 12/08/18 (10.94 ± 5.99 km s ⁻¹), 17/08/18 (low S/N), 18/08/18 (14.49 ± 6.09 km s ⁻¹)
F40	Sinfoni	29/05/13 (-9.57 ± 9.51 km s ⁻¹), 18/06/13 (-3.30 ± 18.00 km s ⁻¹), 17/07/13 (-20.06 ± 11.19 km s ⁻¹), 03/08/13 (-2.71 ± 10.88 km s ⁻¹), 04/08/13 (-0.87 ± 10.08 km s ⁻¹), 06/08/13 (0.90 ± 11.02 km s ⁻¹), 08/08/13 (-18.25 ± 14.85 km s ⁻¹), 26/04/17 (18.17 ± 11.69 km s ⁻¹), 30/04/17 (19.44 ± 9.69 km s ⁻¹), 23/06/17 (-28.02 ± 10.18 km s ⁻¹), 27/07/17 (19.52 ± 9.07 km s ⁻¹), 07/05/18 (-5.06 ± 10.54 km s ⁻¹), 07/08/18 (-4.57 ± 14.84 km s ⁻¹), 12/08/18 (8.52 ± 12.17 km s ⁻¹), 18/08/18 (25.86 ± 11.06 km s ⁻¹)

APPENDIX C: THE X-RAY AND BINARY PROPERTIES OF WNLH STARS

In order to better understand the Arches binaries it is instructive to contrast their properties with those of other known binary populations. Young massive clusters provide the perfect laboratory to undertake such a comparison, since their ensemble properties allow for constraints to be placed on their distances, extinction and ages, in turn aiding the determination of properties such as luminosity for individual members. Moreover, selection effects may be more easily understood and controlled in such an environment. When assessing the binary fraction of clusters, multi-epoch spectroscopic surveys clearly represent the most powerful methodology available, especially if combined with photometric observations. However not all the clusters that host WNLha stars have been subject to such an approach, and in such cases X-ray observations - which are sensitive to the signature of shocked material generated by wind collisions - are an excellent substitute.

In order to undertake such an assessment, the X-ray properties of both single and binary WNLh stars must first be quantified. Clark et al. ((2009)) presented such a summary; however a reappraisal is timely, and we provide that here. For the reasons described above, stars located within stellar aggregates form a ‘gold standard’; moreover many more such regions have now been subject to targeted X-ray investigation (Sect. C.1.1 and refs. therein). Nevertheless, we supplement the resultant sample with the remaining, isolated examples for which suitable data exist, an inclusion driven by the possibility of better understanding the intrinsic multi-wavelength properties of single stars (Sect. C.1.2). For the avoidance of bias, we emphasise that the isolated stellar cohort are not included in the subsequent determination of binary fractions. We also highlight that a large number of WNLha stars have been identified within the the central molecular zone of the Galaxy (Clark et al. (2021)). Unlike the cohorts listed above these were in large part identified via X-ray observations; as a consequence of the obvious resultant bias towards detecting colliding

wind binaries we explicitly exclude them from the analysis presented here.

C1 Data collation and presentation

In the following section we present the results of a literature review undertaken to determine both the X-ray and binary properties of WNLha stars, encompassing both isolated galactic examples and the larger population found within star clusters and associations. In order to produce the mostly complete dataset possible, so as to interpret their X-ray behaviour, we also present the preliminary results of tailored model-atmosphere analysis (cf. Sect. 4) of the X-ray bright WNLha stars found within the Galactic clusters Danks 1 and Mercer 81 (Najarro et al. in prep.).

C1.1 WNLh stars within stellar aggregates

Given their rich stellar populations the young massive cluster R136 and its host star forming region 30 Doradus are obvious targets for such an approach. Unfortunately, their location within the Large Magellanic Cloud leads to significant blending in the crowded core regions of R136, and limits spectral analysis to the brightest of the X-ray sources. As a consequence we also review the contents of Galactic clusters, following the compilation of Rate et al. ((2020b)). From an initial sample of 19 candidate clusters, a number were rejected due to spectral re-classification of relevant cluster members on the basis of published data¹⁰ and/or the cluster population suggesting an age at which, by analogy with the Quintuplet and Westerlund 1 (Clark et al. (2018b), (2020)), core-H burning WNLha stars should not

¹⁰ Cl 1813-178 (Messineo et al. (2011)) and VVV CL009 (Chen e et al. (2013)).

be present¹¹. Four further clusters host WNLha stars but lack the multi-epoch spectroscopic, X-ray and radio observations required to identify binaries¹². This left ten clusters hosting WNLha stars for which the requisite observational data were available, in addition to R136 and 30 Dor¹³. The binary and X-ray properties of the WNLh (and related) stars in these clusters are summarised in Tables C.1 and C.2, while the thumbnail sketches below present a synopsis of the physical properties in each aggregate, including relevant references and conclusions derived from the reported observations.

- **R136:** Schnurr et al. ((2009b)) undertook the most comprehensive RV survey of the six WN5h stars within R136 to date, but report only a single potential binary - R136c - with a tentative ~ 8.4 d period (noting the survey was only sensitive to periods $\lesssim 40$ d). X-ray observations reveal that it is one of the brightest objects within the LMC and demonstrates a hard spectrum (Table C1); strongly suggestive of a colliding wind binary (see below). Of the remaining WN5h stars within R136, Townsley et al. ((2006)) report a blend of emission from R136a1+a2 and R136a3+a6 (the latter being O2 If; Crowther et al. (2016)). Both composite sources are luminous and hard, noting that only single temperature models were employed due to data quality (Table C1). Finally, R136b is heavily blended with other core stars and so is not discussed further, while no mention is made of R136a5 by these authors.

- **30 Doradus:** A further 15 WNLh and related stars are found within the wider confines of 30 Dor (Crowther et al. (2016)). Of these, seven have been confirmed as binaries via spectroscopic observations¹⁴; one is an RV variable but lacks an orbital solution¹⁵; three appear to lack RV variability¹⁶; and appropriate datasets are lacking for four¹⁷ (Table 3, Schnurr et al. (2008b), Bestenlehner et al. (2011), Tehrani et al. (2019)). X-ray data have been presented for a number of these stars, resulting in eight detections. Of these six arise from confirmed binaries/RV variables (Table C1). The most comprehensive analyses are of Mk34 and RMC144. Pollock et al. ((2018)) show that the former is an extremely luminous source (median $L_X \sim 10^{35}$ ergs⁻¹) that is modulated on the orbital period, with a spectrum comprising soft and hard components. Despite having similarly luminous components RMC demonstrates a much more modest X-ray flux, although it too displays orbital modulation and an intrinsically hard spectrum (Townsley et al. (2006), Shenar et al. (2021)). Two further stars - RMC140b and RMC145 - are also luminous and hard sources ($L_X \sim 10^{33} - 10^{34}$ ergs⁻¹; $kT \gtrsim 1.6$ keV; noting that only single temperature models were employed by Townsley et al. (2006)). Mk37, the remaining binary detection, and the RV variable Mk35 are similarly luminous, while RMC134 - which appears not to

be RV variable - is comparatively faint; unfortunately no spectral information is available for any of these three stars (Table C1; Schnurr et al. ((2008b))). Finally, Mk39 has yet to be subject to RV monitoring, but has X-ray properties directly comparable to confirmed binaries (Table C1; Townsley et al. (2006)); Schnurr et al. ((2008b)) returned individual upper limits for the last two binaries (Mk30 and RMC135; Table C1). This leaves a total of five stars for which we adopt the generic detection threshold of 10^{33} ergs⁻¹ reported by Townsley et al. ((2006)) as upper limits, noting that in practice deviations from this are expected depending on the local environment of individual stars.

- **Bochum 7:** Bo7 hosts a single WN8h star, WR12, for which Fahed & Moffat ((2012)) present a spectroscopic orbital solution. Pollock et al. ((1995)) report an X-ray detection, albeit of low detection significance ($(10 \pm 5) \times 10^{32}$ ergs⁻¹ for a distance of 6 kpc, subsequently quoted by Ignace et al. (2000)). However more recent and sensitive observations by Nazé et al. ((2020)) failed to detect it (Table C1), the authors noting that it was observed at a phase at which the WNLha primary and its dense stellar wind would have (partially) obscured the secondary and any putative colliding wind region (see also WR22 below). Clearly future observations will be required to ascertain the nature of its (variable?) emission although we adopt the upper limit of Nazé et al. ((2020)) in this work.

- **Westerlund 2:** Two WNLha stars have traditionally been associated with Wd2; WR20a (WN6ha+WN6ha) and WR20b (WN6h). The former is a well known massive eclipsing system (Rauw et al. (2005); Table 3) and is also a luminous, hard X-ray source that varies on the orbital period (Nazé et al. (2008)); in Table C1 we list the properties for the brightest of the epochs presented by the authors. They further demonstrate that WR20b is a fainter, harder source (representative $L_X \sim 2 \times 10^{33}$ ergs⁻¹, $kT \sim 3.6$ keV) although Skinner et al. ((2010)) prefer a two-temperature fit resulting in a higher luminosity (see Table C1). As a consequence they propose that WR20b is also a colliding wind system; however spectral monitoring by Rauw et al. ((2011)) apparently excludes short binary periods (< 50 d - subject to the usual *caveats* regarding unfavourable orbital inclination). Three further WNLha stars are found in the periphery of Wd2, for which a physical association is currently uncertain: WR20aa (O2If*/WN6), WR20c (O2If*/WN6ha), and WR21a (O3If*/WN6ha+O3V). The very massive short period binary WR21a (Table 3) is, as may be anticipated, a highly luminous, hard and periodically variable X-ray source (Gosset & Naze (2016)). WR20aa and WR20c are possible runaways originating from Wd2 (Roman-Lopes et al. (2011)). Townsley et al. ((2019)) report that the former appears to be a moderately bright and soft X-ray source (Table C1), while no X-ray data are available for the latter. In neither case has RV spectral monitoring been attempted.

- **Carina:** The Carina star-forming complex, encompassing the young massive clusters Trumpler 16 and Collinder 229, is host to three WNLha stars - WR22 (=HD92740A; WN7+abs +09), WR24 (=HD93131; WN6ha), and WR25 (=HD93162; O2.5 If*/WN6 + O). X-ray observations have been made of all three systems (Gosset et al. (2009), Skinner et al. (2010), Raassen et al. (2003), Pollock & Corcoran (2006)) and are summarised in Table C1. WR22 and WR25 have already been confirmed as binaries via RV studies, and both sources also appear to show orbitally modulated X-ray fluxes (Gosset et al. (2009), Arora et al. (2020)). WR22 is of particular interest since it is observed to be particularly faint at the point at which the WNLha and associated wind might be expected to eclipse both the secondary and any associated wind interaction zone ($L_X \sim 6.3 \times 10^{31}$ erg⁻¹). Finally, while spectroscopic evidence for binarity

¹¹ The Quartet (Messineo et al. (2009)), VVV CL036, VVV CL074, and VVV CL099 (Chené et al. (2013)).

¹² [DBS2003]-179 (WR84-1, WR84-6, and WR84-7; Borissova et al. (2012)), VVV CL041 (WR62-2; Chené et al. (2015)), VVV CL073 (WR75-26; Chené et al. (2013)), and Mercer 23 (WR125-3; Hanson et al. (2010))

¹³ While 13 WNLha stars, including the binary CXOU J1745-28, have currently been identified within the Central Molecular Zone of the Galaxy (Mikles et al. (2006), Clark et al. (2009)) we do not consider them here since a large number have been selected on the basis of their X-ray properties, potentially biasing the sample towards colliding wind binaries.

¹⁴ Mk30 (O2 If/WN5), Mk34 (WN6(h)), Mk37 (O3.5 If/WN7), RMC135 (WN6h), RMC140b (WN5h), RMC144 (WN5-6h), and RMC145 (WN6h).

¹⁵ Mk35 (O2 If/WN5).

¹⁶ Mk51 (O3.5 If/WN7), RMC134 (WN6(h)), and VFTS682 (WN5h).

¹⁷ Mk37Wb (O2 If/WN5), Mk39 (O2.5 If/WN6), RMC146 (WN5ha), and RMC147 (WN5h).

Table C1. The X-ray properties of WNha stars in 30 Doradus and galactic clusters

Cluster	Dist. (kpc)	ID	log (L_{bol}/L_{\odot})	L_x (10^{32}ergs^{-1})	kT_1 (keV)	kT_2 (keV)	log (L_x/L_{bol})
R136	~ 50	R136a1	6.94 ^a	100	-	1.2	-
		+a2	6.63 ^a				
		R136a3	6.58 ^a	70	-	4.2	-
		+a6	6.52 ^a				
30 Dor	~ 50	R136c*	6.75 ^a	700	-	3.0	-5.5
		Mk30*	6.16 ^a	< 10	-	-	< -6.8
		Mk34*	6.70 ^b	1000	1.2	4.5	-5.3
		Mk35	6.3 ^a	10	-	-	-6.9
		Mk37*	6.48 ^a	100	-	-	-6.1
		Mk37Wb	6.21 ^a	< 10	-	-	< -6.8
		Mk39	6.4 ^a	130	-	2.0	-5.9
		Mk51	6.2 ^a	< 10	-	-	< -6.8
		RMC134	6.2 ^a	7	-	-	-7.0
		RMC135*	6.2 ^a	< 6.3	-	-	< -7.0
		RMC140b*	6.4 ^a	30	-	2.5	-6.5
		RMC144*	6.72 ^c	25	-	2.1	-6.9
		RMC145*	6.5 ^a	19	-	1.6	-6.8
		RMC146	6.29 ^a	< 10	-	-	< -6.9
RMC147	6.36 ^a	< 10	-	-	< -7.0		
Arches	~ 8	VFTS682	6.51 ^a	< 10	-	-	< -7.1
		F6*	6.32 ^d	110	-	2.2	-5.9
		F7*	6.27 ^d	72	-	1.8	-6.0
		F9	6.15 ^e	46	-	2.5	-6.1
Bochum 7	~6.0	WR12*	5.98 ^f	< 0.4	-	-	< -8.0
Westerlund 2	~ 4.2	WR20a*	6.3 ^g	57	0.4	1.6	-6.1
		WR20b	-	120	0.4	5.4	-
		[WR20aa	-	24	0.9	-	-]
		[WR21a*	-	194	0.8	3.0	-]
Carina	~ 2.6	WR22*	6.35 ^f	4.2	0.6	2.0	-7.3
		WR24	6.19 ^f	6.4	0.7	3.3	-7.0
		WR25*	6.61 ^f	84	0.6	2.7	-6.3
NGC 3603	~ 7.6	WR43A*	6.39 ^h	360	0.8	3.1	-
		+WR43B	6.46 ^h				
		WR43C*	6.35 ^h	260	1.0	7.9	-5.5
		[WR42e	-	2.3	-	-	-]
		[WR43-2*	-	2.9	-	-	-]
Danks 1	~ 3.8	WR48-8	5.44 ^e	17	-	-	-5.8
		WR48-9	5.99 ^e	43	-	-	-6.0
		WR48-10	5.70 ^e	14	-	-	-6.2
Mercer 81	~ 10	WR76-3	6.17 ^e	14	-	2.0	-6.6
		WR76-7	6.39 ^e	35	-	2.6	-6.4
Sco OB1	~2	WR78*	5.8 ^f	6.9	0.6	2.3	-6.6
		WR79a*	5.78 ⁱ	1.4	0.6	2.7	-7.2
HM-1	~ 3.3	WR87	6.21 ^f	1.6	-	2	-7.6
		WR89*	6.33 ^f	154	0.6	2	-5.7
W43	~ 6	WR121a*	-	154	1.0	3.6	-

Sources in the vicinity of the clusters but for which a physical association has yet to be proved are given in square brackets. Identifiers marked with an asterisk are those which are identified as binaries via optical or IR observations, non-thermal radio emission (WR78 and WR89) or periodically modulated X-ray activity (WR121a). Variable X-ray sources have their representative fluxes given in italics. Parameters for R136a1+a2, R136a3+a6 and WR43A+WR43B represent a blend of both sources (see text for further details). References for the X-ray properties are given in the body of the text, while those for the bolometric luminosities of the system primaries are ^aCrowther et al. ((2016)), ^bTehrani et al. ((2019)), ^cShenar et al. ((2021)), ^dthis work, ^eNajarro et al. (in prep.), ^fHamann et al. ((2019)), ^gRauw et al. ((2005)), ^hCrowther et al. ((2010)), and ⁱCrowther & Bohannan ((1997)). We highlight that Mk34, RMC144, and WR20a are composed of two 'twins' - as with other systems the bolometric luminosities presented are those of the combined binary; individual components in these systems will be 0.3dex fainter. Finally we have scaled the bolometric luminosities for WR24, WR24, and WR25 (Hamann et al. ((2019)) to a common distance of 2.6kpc for the Carina complex.

Table C2. The X-ray properties of isolated WNha stars

ID	Dist. (kpc)	log (L_{bol}/L_{\odot})	L_{x} (10^{32}ergs^{-1})	log ($L_{\text{x}}/L_{\text{bol}}$)
WR16	2.6	5.72 ^a	0.13	-8.2
WR29 ^{b*}	6.0	5.73 ^b	2 - 3	-7.1 - -6.9
WR40	4.0	5.91 ^a	< 0.7	< -7.7
WR105 ^{a*}	1.8	5.89 ^a	4 - 12	-6.9 - -6.4
WR148 ^{a*}	8.3	6.3 ^{a,c}	2.1	-7.6

Identifiers marked with an asterisk are those which are identified as binaries via optical (WR29 and WR148) and radio (WR105) observations. References for the X-ray properties are given in the body of the text, while those for the bolometric luminosities of the system primaries are ^aHamann et al. ((2019)), ^bNaze et al. ((2020)) and ^cZhekov ((2017)). Note the X-ray luminosities listed for WR29 and WR105 represent the range allowed under the modelling assumptions of Naze et al. ((2020)).

is lacking for WR24, we highlight the close similarity of its X-ray properties to those of WR22.

- **NGC 3603:** Three WNLha stars are found within the core of NGC3603 - WR43A (= cl* NGC 3603 BLW A1; WN6ha+WN6ha), WR43B (= cl* NGC 3603 MDS B; WN6ha) and WR43C (= cl* NGC3603 MDS C; WN6ha + ?), of which WR43A and WR43C are known short period binaries (Table 3). X-ray observations are complicated by blending due to the compact nature of NGC3603 but Moffat et al. ((2002); their Fig. 4) suggest fluxes of $L_{\text{x}} \sim 10^{33}\text{ergs}^{-1}$ for WR43B, $L_{\text{x}} \geq 4 \times 10^{34}\text{ergs}^{-1}$ for WR43C and $L_{\text{x}} \geq 10^{34}\text{ergs}^{-1}$ for the blend comprising WR43A, cl* NGC3603 BLW A2 (O3 V) and cl* NGC3603 BLW A3 (O3 III(f*)); unfortunately no spectral information was presented for any source. Subsequently, Huenemörder et al. ((2009)) analysed the emission spectra deriving from a blend of WR43A+WR43B and from WR43C, finding both to be highly luminous and demonstrating hard spectral components (cf. Table C1). Of these Pollock et al. ((2018)) report WR43C as being variable. Two further WNLha stars are located in the surrounds of NGC3603. Displaced $\sim 6\text{pc}$ from the cluster core, Roman-Lopes ((2012)) suggests that the O2 If*/WN6h stars WR42e could be a runaway (and hence single); nevertheless they report a X-ray luminosity that is comparable with the binary WR22 (Table C1) but no spectral information. Finally WR43-2 (= cl* NGC3603 MTT 58; O2-3.5 If*/WN5-6ha + ?) is located within a compact H II region on the periphery of the wind-blown bubble encompassing NGC3603, some $\sim 2\text{pc}$ distant from the cluster core. Again lacking spectral information, it is of comparable luminosity to WR42e (Roman-Lopes (2013)), but is unambiguously a short-period binary on the basis of periodic photometric modulation (Jaque Arancibia et al. (2015)).

- **Mercer 30:** de la Fuente et al. ((2016)) report two WNLh stars within the cluster Mercer 30 - WN46-5 (= [DNB2016] Mc30-7; WN6h) and WN46-6 (= [DNB2016] Mc30-8; WN7h), which modelling suggests are highly luminous, and hence massive ($\log L/L_{\odot} \geq 6.0$ and $M_{\text{current}} \geq 50M_{\odot}$). Despite a limited dataset comprising three epochs of spectroscopic observations, the former is clearly a binary by virtue of $\Delta RV \sim 191\text{km s}^{-1}$ between observations in 2009 and 2011; unfortunately no X-ray observations exist for this cluster.

- **Mercer 81:** Davies et al. ((2012a)) and de la Fuente et al. ((2013)) report five WN7-8ha stars within the distant and highly reddened cluster Mercer 81; WR76-9 (= [DDN2012] 3), WN76-6 (= [DDN2012] 7), WR76-2 (= [DDN2012] 5), WR76-7 (= [DDN2012] 2), and WR76-3 (= [DDN2012] 8). No radial velocity surveys have been undertaken but the X-ray survey of Norma Arm by Rahoui et al. ((2014)) report detections WR76-3 and WR76-7

(their sources #1278 and #1279 respectively), finding them to be hard, bright sources (Table C1; assuming a single temperature fit). Bolometric luminosities for the two X-ray detections derive from quantitative modelling to be presented in Najarro et al. (in prep.); we find both stars to be intrinsically highly luminous (Table C1).

- **Danks 1:** In the absence of RV observations, Zhekov et al. ((2017)) presents a preliminary analysis of X-ray data, quoting fluxes for the three WNLha stars WR48-8 (= [DCT2012] D1-5; WN8-9ha), WR48-9 (= [DCT2012] D1-1; WN8-9ha), and WR48-10 (= [DCT2012] D1-2; WN8-9ha), with Townsley et al. ((2019)) subsequently reporting that the first two sources are variable, with fluxes decreasing by factors of ~ 5 and ~ 10 respectively, between two epochs of observations separated by $\sim 4\text{yr}$. While neither author presents spectral information for these detections both conclude that they are bona fide binaries based on their X-ray properties (a claim we revisit below). As with Mercer 81 we provide bolometric luminosities for the three X-ray detections derived from modelling in Table C1 (Najarro et al. in prep.). We highlight that while WR48-9 and 48-10 are broadly comparable to other Galactic examples, WR48-8 is significantly fainter, while the emission lines in the K-band spectrum appear anomalously broad and weak (Davies et al. (2012b)). As a consequence we suspect its nature and/or evolutionary pathway differs from other examples; we return to this topic in Najarro et al. (in prep.).

- **Havlen Moffat 1;** As with Danks 1, HM-1 as a whole has yet to be subject to a systematic, modern RV survey, and so we are forced to fall back on observations at other wavelengths; WR89 (WN7h) appears to be a non-thermal radio source and hence colliding wind binary (Cappa et al. (2004)), although inspection of archival spectra fails to reveal RV shifts (Nazé et al. (2013))¹⁸. Nevertheless, these authors reveal it to have an extreme (variable) X-ray luminosity and a spectrum comprising both soft and hard thermal components. Unfortunately, only X-ray observations are available to determine the nature of WR87 (WN7h); while it is comparatively faint with respect to WR79a, it too has a hard spectral component at least consistent with emission from a wind collision zone (Table C1 and discussion below).

- **Sco OB1:** Hosting the young massive cluster NGC6321 at its core, the Sco OB1 association contains two WNLh stars - WR 78 (= NGC 6231 305; WN7ha) and WR79a (= NGC6231 327; WN9ha) - that, in contrast to many other examples considered, demonstrate relatively modest bolometric luminosities Table C1). Both stars are detected at X-ray energies, and share similar properties, being rather faint and hard sources (Skinner et al. (2010), (2012)). WR78 appears to demonstrate aperiodic optical variability (Skinner et al. (2012) and refs. therein) while Chini et al. ((2012)) lists WR79a as an SB2 system but provides no links to an appropriate reference; as such, we refrain from assuming binarity for either on the basis of these works. However de Becker & Ruacq ((2013)) and Cappa et al. ((2004)) report that both stars are non-thermal radio sources and hence colliding-wind binaries: a conclusion we adopt for the remainder of this study.

- **W43:** The giant H II region hosts a young, heavily embedded cluster at its core, which in turn contains a single WN7ha star: WR121a. Arora & Pandey ((2020)) provide an analysis of time-resolved X-ray observations of this star, finding it to be a hard and highly luminous source, which demonstrates an apparent $\sim 4.1\text{d}$ periodicity that they attribute to orbital modulation in a massive compact binary. Examining near-IR and radio data, Luque-Escamilla et al.

¹⁸ The lack of spectral variability is potentially explicable by unfavourable inclination and/or a long or highly eccentric orbit.

((2011)) further show that WR121a maybe resolved into two components separated by a projected angular distance of $\sim 0.6''$, suggesting the possible presence of a further stellar companion.

- **Quintuplet:** Finally we turn to the Quintuplet, which Clark et al. ((2018b)) report contains two WN8-9ha (qF256 and qF274) and an hybrid O7-8 Ia⁺/WN8-9ha star (LHO001). Given the remaining cluster population their presence is a surprise, with the authors suggesting they could be the result of binary interaction. Unfortunately only LHO001 has been the subject of multi-epoch spectroscopy, which reveal it to be highly variable, although insufficient data exists to attempt to identify periodic modulation. Wang et al. ((2006)) present X-ray observations of the Quintuplet; none of these sources are detected and, as with the Arches (Sect. 3.2.1), a combination of potential blending and the presence of spatial variable diffuse emission prevent the derivation of upper limits. Given the limited observational data for these stars as well as their uncertain provenance, we refrain from discussing them further.

C1.2 Isolated WNLh stars

We may supplement the above dataset with five isolated single and binary stars. Of the former, Skinner et al. ((2012)) report a detection of the WN8h star WR16; unfortunately it is too faint for spectral analysis (Table C2, with the flux scaled to the distance adopted by Hamann et al. (2019)). Although optically variable it currently cannot be unambiguously identified as a binary (Antokhin et al. (1995)). Similar conclusions are also reported for WR40 (WN8h) by these authors; unfortunately Gosset et al. ((2009)) are only able to provide a (conservative) upper limit to the X-ray flux which, suitably scaled, is repeated in Table C2. Turning to the binaries, Nazé et al. ((2020)) find WR29 (WN7h+O; Table 3) to be a faint X-ray source; assuming a canonical $kT \sim 0.6 + 6.9\text{keV}$ thermal spectrum it appears moderately luminous ($\sim 2 - 3 \times 10^{32}\text{ergs}^{-1}$; Table C2). WR105 (WN9h) is a non-thermal radio source (Montes et al. (2009)) and hence a strong colliding wind binary candidate. Although a weak X-ray detection (Nazé et al. (2020)), under the same modelling assumptions adopted for WR29 it appears to be intrinsically luminous ($\sim 4 - 12 \times 10^{32}\text{ergs}^{-1}$; Table C2).

Finally we turn to the runaway binary WR148 (WN8h), the nature of which has been the subject of some debate e.g. Drissen et al. (1986). Recently Munoz et al. ((2017)) have suggested an O5V classification for the secondary; however the canonical mass of such an object - they quote $\sim 37M_{\odot}$ - is in tension with the inclination derived by Drissen et al. ((1986)). Upon reappraisal of the relevant photometric and polarimetric data the former authors suggest that the results are ‘inconclusive’. Allowing for a lower inclination, the canonical mass of the O5V secondary implies a current mass of $\sim 33M_{\odot}$ for the WN7ha primary - unexpectedly low in comparison to other examples (Table 3) and for a luminosity of $\sim 10^{6.3}L_{\odot}$ ¹⁹. Nevertheless, Zhekov ((2012)) report a rather moderate X-ray luminosity ($\sim 2.1 \times 10^{32}\text{ergs}^{-1}$) and a thermal spectrum ($kT \sim 0.4 + 1.0\text{keV}$) for the system.

For completeness we briefly discuss the Galactic centre source CXO J174536.1-285638 (WN9ha). Although excluded from the sample for the reasons given above, we note that it is a long period binary (~ 189 d; Mikles et al. (2008)). Adopting a two-component spectral fit ($kT \sim 0.7 + 4.6\text{keV}$) implies an exceptional X-ray luminosity

¹⁹ Obtained by scaling the luminosity of Hamann et al. ((2019)) to the consensus distance of 8.3kpc (Zhekov (2012)), noting that Rate & Crowther ((2020a)) suggest $\sim 9.47_{-1.49}^{+1.77}$ kpc.

($L_X \sim 10^{35}\text{ergs}^{-1}$) that is directly comparable to that of Mk34 (Table C1). This indicates that the latter is not a pathological system; however, the lower luminosity of the primary ($L_{\text{bol}} \sim 10^{6.24}$; Clark et al. (2009)) leads to an even more extreme $\log(L_X/L_{\text{bol}}) \sim -4.8$ for CXO J174536.1-285638 than was found for Mk34 (Table C1).

C2 Data interpretation

C2.1 The X-ray properties of WNLh stars

Historically, and by analogy to O stars, WR binaries have been expected to be hard, overluminous X-ray sources. However recent studies suggest that such a picture may be overly simplistic. In particular, while a number of confirmed O star and WR binaries within Wd1 conform to this expectation, others are found to have comparatively soft spectra consistent with emission from single stars (Clark et al. (2019c); see also Oskinova (2015), (2016)). Considering a dataset exclusively comprising WR stars allowed Skinner et al. ((2010), (2012)) to report the ubiquity of a hard ($kT \gtrsim 2\text{keV}$) component in the X-ray spectra of all WN stars with spectra sufficient to accommodate modelling. Conversely, Oskinova ((2016)) state that, on average, single WN stars display a softer ($kT \sim 0.4\text{keV}$) spectrum. Clearly, reconciling these potentially conflicting findings requires an accurate determination of the binary properties of the stars studied. Nevertheless, studies focusing on individual binary systems via multi-epoch, phase-resolved observations indicate that where present - and as with O stars - the high-temperature spectral component originates in the wind collision zone (e.g. Gosset et al. (2009), Montes et al. (2013), Parkin & Gosset (2011)).

Mindful of the fact that the cohorts considered by Skinner et al. ((2012)) and Oskinova ((2015), (2016)) comprise in part H-free WNE stars - and so are not directly comparable to our sample - we highlight that the spectral properties of the WNLh stars considered here are uniformly characterised by the presence of a hard thermal component (Table C1), potentially indicative of binarity. However, while the possibility remains that single WR stars may also demonstrate similarly hard X-ray spectra (Skinner et al. (2012)) it appears premature to utilise this observational feature to unambiguously identify WR binaries.

This leaves X-ray luminosity as a prospective binary diagnostic. Oskinova ((2015)) and Gagné et al. ((2012)) provide compilations of X-ray properties for single and binary WRs, finding that the luminosities of both show an exceptional variance, spanning \sim four orders of magnitude. Nevertheless, they identify *potential* trends whereby (i) binaries appear to be more prevalent amongst the brighter X-ray sources, apparently obeying the canonical $L_X/L_{\text{bol}} \sim 10^{-7}$ relationship delineated by hot, massive stars and (ii) the most luminous systems are biased towards the binaries with the longest periods. However, interpretation is complicated by the heterogenous nature of the samples appraised by these authors, comprising both WNLh and the more evolved H-free ‘classical’ WNE stars (with the latter being of systematically lower luminosity).

Motivated by their evolutionary uniformity we plot L_{bol} versus L_X for our sample of WNLh stars in Fig. C.1 (c.f. Tables C.1 and C.2; note that due to uncertainty regarding individual contributions, the blended R136 and NGC3603 sources are not included). For consistency, in all instances we plot the integrated bolometric luminosity of the stellar system in question (with that of F9 obtained via an identical methodology to that described in Sect. 4; Najarro et al. in prep.). It is expected that for the majority of objects considered this will be equivalent to the output from the WNLh star that dominates the emergent spectrum. However at least three systems - WR20a, MK34

and RMC144 - are known binaries comprising twin WNLh stars; in such cases the luminosity of individual components is ~ 0.3 dex lower than represented in Fig. C.1. We find that X-ray luminosities of the stars range over four orders of magnitude: from $\sim 10^{31}$ ergs $^{-1}$ (for the apparently single WR16) to $\geq 10^{35}$ ergs $^{-1}$ (the binaries Mk34 and CXO J174536.1-285638), the latter stars being amongst the most luminous colliding-wind systems known (Gagne et al. (2012)). Despite considerable scatter, a positive trend between X-ray and bolometric luminosities is apparent. With 23/39 of the WNLh stars considered exceeding the empirical $L_X/L_{\text{bol}} \sim 10^{-7}$ relationship found for O stars, it appears that the former have a systematically greater X-ray luminosity than the latter. Moreover there are hints that the correlation is also steeper for WNLh stars, with 12/15 examples with $\log(L_{\text{bol}}/L_{\odot}) > 6.3$ exceeding this threshold (Fig. C.1).

Of the remaining stars, the constant RV sources WR24 and R134 essentially straddle this division²⁰, while the upper limits to the X-ray flux of five stars - the binary Mk30 and apparently single star Mk51 as well as MK37Wb, RMC146, and RMC147 (which are currently of indeterminate nature) - render their placement uncertain. Indeed, only nine stars are unambiguously found below this threshold; these comprise the *apparently* single stars WR16, WR40 and VFTS682; the binaries WR12, WR22, WR79a, WR148 and RMC135; and WR87, the nature of which is currently uncertain.

Of these the binaries WR12 and WR22 are of particular interest given the stringent upper limits obtained for their X-ray fluxes ($L_X \leq 10^{31.8}$ ergs $^{-1}$; Fig. C.1). These derive from observations of both systems obtained at orbital phases when their WNLh primaries potentially obscure their companions and any putative wind collision zones. Following the arguments of Gosset et al. ((2009)) and Nazé et al. ((2020)), one might expect the dense, metal-rich winds of the WNLh stars to efficiently absorb high energy emission from the latter components, leaving only their own intrinsically weak emission visible. Indeed, the observations of both WR16 and WR40 support the hypothesis that single WNLh stars are particularly faint X-ray sources.

A corollary of this hypothesis would be that all of the X-ray luminous WNLh stars are colliding wind binaries. Indeed 16 of the 21 confirmed WNLh binaries²¹ are found above the $L_X/L_{\text{bol}} \sim 10^{-7}$ threshold; of the remaining seven co-located stars six currently lack diagnostic observations²² and only Arches F9 shows no evidence for binary-induced RV variability at this time (although we note that its radio properties are indicative of binarity; Sect. 3.2). Thus we might infer a binary fraction of 15/16 ($\sim 94\%$) amongst stars exceeding this limit at this time (and a minimum of $\sim 70\%$ if the remainder are found to be single).

Consequently, we adopt $L_X/L_{\text{bol}} \sim 10^{-7}$ as a conservative and empirical lower limit for the identification of colliding wind binaries with WNLh primaries via their X-ray emission. In doing so we reiterate that five known binaries fall below this threshold; however lowering the limit to encompass all these system at all times would potentially permit the inclusion of genuinely single stars. This is evident upon consideration of the variable X-ray emission from the binaries WR12 and WR24, which appear to manifest as single stars at certain orbital phases. In addition to their intrinsic variability, the large variance in the X-ray properties of binaries likely results from

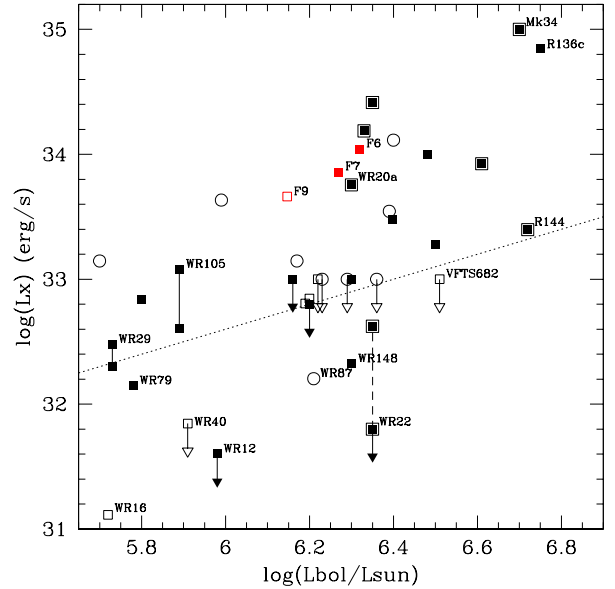


Figure C1. Plot of bolometric and X-ray luminosities for the WNLh stars given in Tables C.1 and C.2 (black), with the addition of the Arches detections F6, F7, and F9 (red symbols). Confirmed binaries (including the RV variable Mk35 for simplicity) are given by filled squares, stars with no indication of binarity are depicted by open squares, and the subset for which the requisite observations have yet to be undertaken represented by open circles. Stars known to be X-ray variable are indicated by the nested symbols. The second, open symbol for W22 represents the upper limit to the intrinsic emission from the WN7h primary according to Gosset et al. ((2009)). The solid lines joining the two points for WR29 and WR105 indicate the range of possible luminosities for both stars (Nazé et al. (2020)). Luminosities are shifted slightly for RMC140b (-0.003 dex), RMC144 (+0.003 dex), Mk51 (+0.02 dex) and Mk37Wb (+0.02 dex) to aid clarity. The canonical $L_X = 10^{-7} L_{\text{bol}}$ relationship that Oskoina ((2015)) suggests is followed by O and WN stars is given by the dotted line; stars falling below this limit are individually labeled, as are certain additional stars of interest (subject to figure clarity). Finally the low luminosity star WR48-8 is not plotted, but lies significantly above the threshold.

the diversity of their physical properties - in particular the nature of the secondary, orbital separation and eccentricity (Gagné et al. (2012) and Table 3) - which may allow some systems to remain inherently faint. That the absolute X-ray luminosity of binaries with WNLh primaries appears greater than that of those containing O stars likely reflects the difference in wind properties, with the former supporting more powerful, optically thick winds in comparison to the optically thin outflows of the latter (e.g. Gräfener ((2021))).

C2.2 The binary fraction of WNLh stars within clusters

How may we interpret these data in terms of the incidence of binarity and the X-ray properties of such systems? Regarding the frequency of occurrence, as a first step we may simply consider those stars that appear unambiguously binary via spectroscopic determination of an orbital period. Mindful of the limitations of extant RV and X-ray surveys, we find 9/17 ($\sim 53\%$) confirmed binaries within R136/30 Dor (including the RV variable Mk35). Likewise, recognising that clusters such as Danks 1, HM-1 and Mercer 81 have yet to be subject to systematic RV surveys (and the limited nature of the Mercer 30 study) we arrive at a total of 7/11 in five galactic aggregates (Table C2;

²⁰ Based on the results presented in Fig. 4 of Moffat et al. ((2002)), WR43B also lies on this threshold which, based on the values in Table C1 would imply that WR43A significantly exceeds it.

²¹ WR20a, WR25, WR29, WR43C, WR78, WR89, WR105, F6, F7, Mk34, Mk35, Mk37, RMC136, RMC140b, RMC144, and RMC145

²² WR48-8, WR48-9, WR48-10, WR76-3, WR76-7, and Mk39

Bochum 7, Westerlund 2, Carina, NGC3603 and Mercer 30). To this tally we may add the periodic X-ray source WR121 (W43) and the non-thermal radio sources WR78 (Sco OB1) and WR89 (HM-1) where emission is thought to arise in shocked material in the wind collision zone, increasing the Galactic count to 10/16. This implies a minimum binary fraction of 19/33 ($\gtrsim 58\%$) before allowance is made for the insensitivity of the extant RV surveys to longer period systems and those seen at unfavourable orbital inclinations.

This brings us to interpretation of the X-ray properties of these stars. Orbitally modulated X-ray emission is apparent in the spectroscopically confirmed binaries Mk34, RMC144, WR20a, WR21a, WR22, and WR25; on this basis the periodically variable X-ray source WR121a is also a compelling binary candidate (see also CXO J1745-28; Table 3). However, many of the remaining candidate and confirmed WNLh binary systems have an insufficient timeline of X-ray observations to permit a search for periodicities. For such systems we adopt $L_X/L_{\text{bol}} \gtrsim 10^{-7}$ as a conservative threshold for binarity; in doing so we are mindful of (i) the relative paucity of observational constraints for apparently *bona fide* single stars, (ii) that genuine binaries may fall below this threshold (cf. Fig. C.1 and Sect. 3.2.2) and (iii) that we may not assess binarity for a number of X-ray detected WNLh stars that currently lack bolometric luminosity determinations²³.

Nevertheless, adopting this discriminant means we may assert binarity for Arches F9 (see Sect. 3.3.2) as well as Mk39 (within 30 Dor), WR48-8, WR48-9, WR48-10 (within Danks 1), and WR76-3 and WR76-7 (Mercer 81). Critically, this would mean recognising the possibility of a binary fraction approaching unity for the most luminous subset of stars ($\log(L_{\text{bol}}/L_{\odot}) > 6.3$; Sect. C.2.1). Such a conclusion, however, is subject to the *caveat* that the nature of some members of the very luminous cohorts within R136 (a1, a2, a3, and a5) and NGC3603 (WR43A and WR43B) remain difficult to ascertain due to blending, although the properties of the respective composite X-ray sources are strongly suggestive of binarity amongst one or more of the component stars (Table C1). More provocatively, if we were to take the observations summarised in Fig. C.1 at face value, one would infer that (apparently) single WNLha stars are intrinsically X-ray faint ($L_X < 10^{32} \text{ergs}^{-1}$). This would lead to the conclusion that all but one of the stars reported as X-ray detections in Table C1 - which, with the exception of WR12, uniformly exceed this value at one or more epochs - are binaries: a verdict consistent with their uniformly hard X-ray spectra.

Nevertheless, under the former, more conservative X-ray cut, the binary count for R136/30 Dor rises to 10/21 ($\sim 48\%$) with the inclusion of Mk39 (noting that the sample size has risen since the full cohort of WNLh stars has been subject to X-ray observations). Similarly, consideration of the additional X-ray diagnostic leads to the identification of 15/24 ($\sim 63\%$) binaries within the ten galactic aggregates considered above. Given the foregoing discussion and the diverse and incomplete nature of the multi-wavelength observations employed in the preceding assessment, we consider it highly likely that the simple number counts presented above are lower limits to the true binary fractions, but the heterogenous nature of the extant datasets means we are unable to assess the degree of incompleteness at this time. We discuss the Arches cluster in the context of these observations - and the resultant conclusions - further in Sect. 4 and 5.

This paper has been typeset from a $\text{\TeX}/\text{\LaTeX}$ file prepared by the author.

²³ WR20aa, WR20b, WR21a, WR42e and WR43-2.